Mechanisms and Models of Cardiac Excitation-Contraction Coupling

R.L. Winslow[1], R. Hinch[2] and J.L. Greenstein[1]

[1] Center for Cardiovascular Bioinformatics and Modeling and The Whitaker Biomedical Engineering Institute, The Johns Hopkins University School of Medicine and Whiting School of Engineering
[2] Mathematical Institute, University of Oxford

1 Introduction

Intracellular calcium (Ca^{2+}) concentration plays an important regulatory role in a number of cellular processes. Cellular influx of Ca^{2+} activates intracellular signaling pathways that in turn regulate gene expression. Studies have identified over 300 genes and 30 transcription factors which are regulated by intracellular Ca^{2+} [1, 2]. Fluctuation of intracellular Ca^{2+} levels is also known to regulate intracellular metabolism by activation of mitochondrial matrix dehydrogenases. The subsequent effects on the tri-carboxylic acid cycle increase the supply of reducing equivalents (NADH, $FADH_2$), stimulating increased flux of electrons through the respiratory chain [3]. Most importantly, Ca^{2+} is a key signaling molecule in excitation-contraction (EC) coupling, the process by which electrical activation of the cell is coupled to mechanical contraction and force generation.

The purpose of this chapter is to review the important role of Ca^{2+} in cardiac EC coupling, with a particular focus on presentation of quantitative models of the EC coupling process. One of the most remarkable features of cardiac EC coupling is that structural and molecular properties at the microscopic scale have a profound influence on myocyte function at the macroscopic scale. Thus, modeling of cardiac EC coupling is confronted with the enormous challenge of needing to integrate diverse information collected at multiple scales of biological analysis into comprehensive models. In this chapter, we will consider three different approaches to such multi-scale modeling of cardiac EC coupling, reviewing the strengths and weaknesses of each approach.

2 The Molecular and Structural Basis of Cardiac EC Coupling

2.1 Structural Basis of EC Coupling

The nature of EC coupling is linked closely to both the micro-anatomical structure of the myocyte as well as the arrangement of contractile proteins within the cell. These relationships are shown in Fig. 1. The basic unit of contraction in the cardiac myocyte is the sarcomere. Individual sarcomeres are approximately $2.0\,\mu$m in length and are bounded on both ends by the Z-disks. The H-Zone contains the thick (myosin) filaments and is the region within which there is no overlap with thin (actin) filaments. The A-band is the region spanned by the length of the thick filaments. The shaded region in Fig. 1 represents the region of overlap of thick and thin filaments. Muscle contraction is accomplished by the sliding motion of the thick and thin filaments relative to one another in this region in response to elevated levels of intracellular calcium (Ca^{2+}) and ATP hydrolysis.
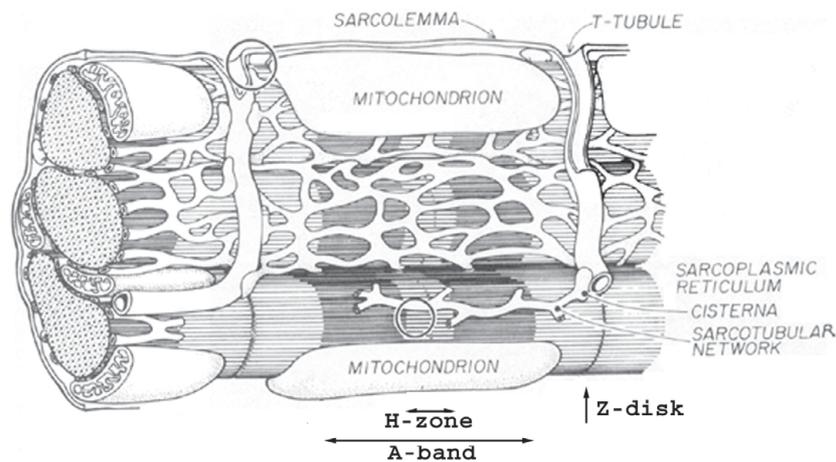

Fig. 1. Ultrastructure of the cardiac ventricular myocyte, illustrating the organization of sarcomeres and the T-tubules. Reproduced from Fig. 1.14 of Katz [73] with permission

Figure 1 also shows that sarcomeres are bounded on each end by the T-tubules [4]. T-tubules are cylindrical invaginations of the sarcolemma that extend into the myocyte (Fig. 2), approaching an organelle known as the sarcoplasmic reticulum (SR). The SR is comprised of two components known as junctional SR (JSR) and network SR (NSR). The NSR is a lumenal organelle extending throughout the myocyte. NSR membrane contains a high concentration of the SR Ca^{2+}-ATPase (SERCA2α) pump, which transports Ca^{2+}
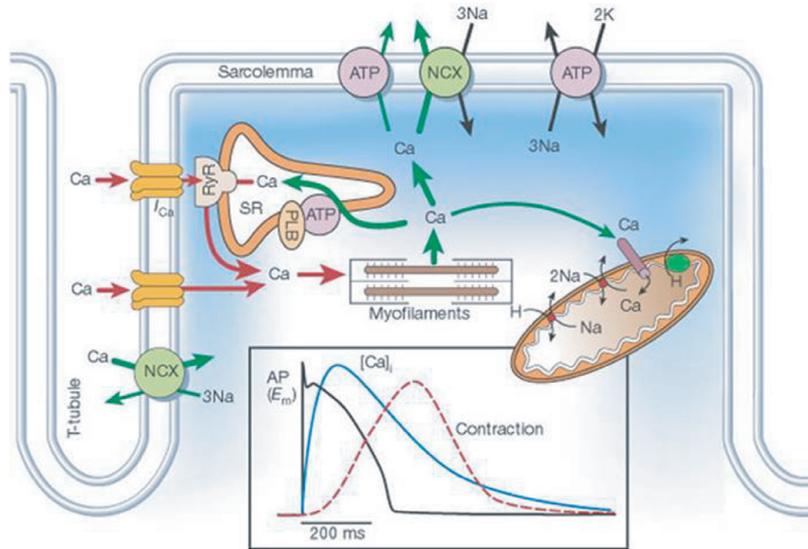
Fig. 2. Illustration of the physical organization and channel localization in the cardiac dyad. Reproduced from Bers Fig. 1 [66] with permission

from the cytosol into the lumen of the NSR (Fig. 2). The JSR is that portion of the SR most closely approximating the T-tubules. The close proximity of these two structures ($\sim$10 nm) forms a restricted region commonly referred to as the "dyad" or "subspace" with an approximate diameter of 400 nm. Ca^{2+} release channels (known as ryanodine receptors or RyRs) are located in the dyadic region of the JSR membrane. In addition, sarcolemmal L-Type Ca^{2+} channels (LCCs) are located preferentially within the dyadic region of the T-tubules, where they are in close opposition to the RyRs. It has been estimated that there are approximately 10 LCCs per dyad [5] and $\sim$50,000 active LCCs per myocyte.

2.2 The Molecular Basis of Cardiac EC Coupling

2.2.1 Properties of LCCs

Cardiac LCCs are multi-subunit protein complexes located in the T-tubular membrane (for review, see [6]). The main functional subunit of the cardiac LCC is the α_{1c} subunit. Each α_{1c} subunit has 6 transmembrane segments (S1-S6) and four subunits assemble to create the LCC pore. LCCs undergo voltage-dependent activation and inactivation. The voltage sensor is located in the S4 segment and the inactivation gate is located in the S6 segment [7]. LCCs are also composed of auxiliary subunits. Four distinct β subunits, with multiple splice variants, bind to the channel complex to modify its properties [8]. An $\alpha_2\delta$ subunit also interacts with and modifies channel properties. Both

the α_{1c} and the β_{2a} subunit (the dominant β subunit isoform in heart) contain protein kinase A (PKA) phosphorylation sites [9].

LCCs also undergo inactivation in response to elevated Ca^{2+} levels within the dyadic space near the inner pore of the channel – a process referred to as Ca^{2+}-dependent inactivation. Inactivation of LCCs is mediated by Ca^{2+} binding to the calmodulin (CaM) molecule which is constitutively tethered to the LCC [10]. Following Ca^{2+} binding, CaM binds to an IQ-like domain located in the carboxyl tail of the α_{1c} subunit. This in turn leads to a conformational change of the EF hand region located downstream from the IQ domain, initiating channel inactivation [11].

An important issue, to be discussed in subsequent sections, is the relative magnitude of voltage- versus Ca^{2+}-dependent inactivation of LCCs. Recent data regarding the relative contributions of these processes are presented in Fig. 3 (adapted from Linz and Meyer, Fig. 11 [12]). Open triangles show the fraction of LCCs not voltage-inactivated and filled circles show the fraction of LCCs not Ca^{2+}-inactivated. Measurements were made in isolated guinea pig ventricular myocytes in response to an action potential (AP) clamp stimulus (upper panel). These data show that the fraction of LCCs not Ca^{2+}-inactivated is small relative to the fraction not voltage-inactivated. Thus, Ca^{2+}-inactivation dominates over voltage-inactivation during the time course of an AP.

Figure 3B shows recent data from the laboratory of David Yue and colleagues (adapted from Fig. 5 of Peterson et al. [10]). The left panel of Fig. 3B shows current through LCCs in response to a voltage-clamp step from a holding potential of $-80\,mV$ to $-10\,mV$. Two current traces are shown, one with Ca^{2+} and one with Ba^{2+} as the charge carrier. Ca^{2+}-dependent inactivation of LCCs is thought to be ablated when Ba^{2+} is used as the charge carrier. The Ba^{2+} current thus reflects properties of voltage-dependent inactivation of LCCs. Comparison of the two current traces suggests that over a time scale of a few hundred milliseconds, Ca^{2+}-dependent inactivation is fast and strong whereas voltage-dependent inactivation is slow and weak. The right panel of Fig. 3B shows results obtained when a mutant CaM incorporating point mutations which prevent Ca^{2+} binding is over expressed in the myocytes, thus definitively ablating Ca^{2+}-dependent inactivation. Under this condition, the Ca^{2+} and Ba^{2+} currents are similar, thus providing an independent measurement confirming that Ca^{2+}-dependent inactivation of LCCs is fast and strong, whereas voltage-dependent inactivation is slow and weak.

2.2.2 Properties of RyRs

Ryanodine receptors (RyRs) are ligand-gated channels located in the dyadic region of the JSR membrane. These channels open following binding of Ca^{2+} in response to elevated Ca^{2+} levels in the dyad, thus releasing Ca^{2+} from the JSR. Cardiac RyRs are composed of four 565-kDa subunits and four 12-kD FK506 binding proteins (FKBP12.6). FKBP12.6 stabilizes the closed state
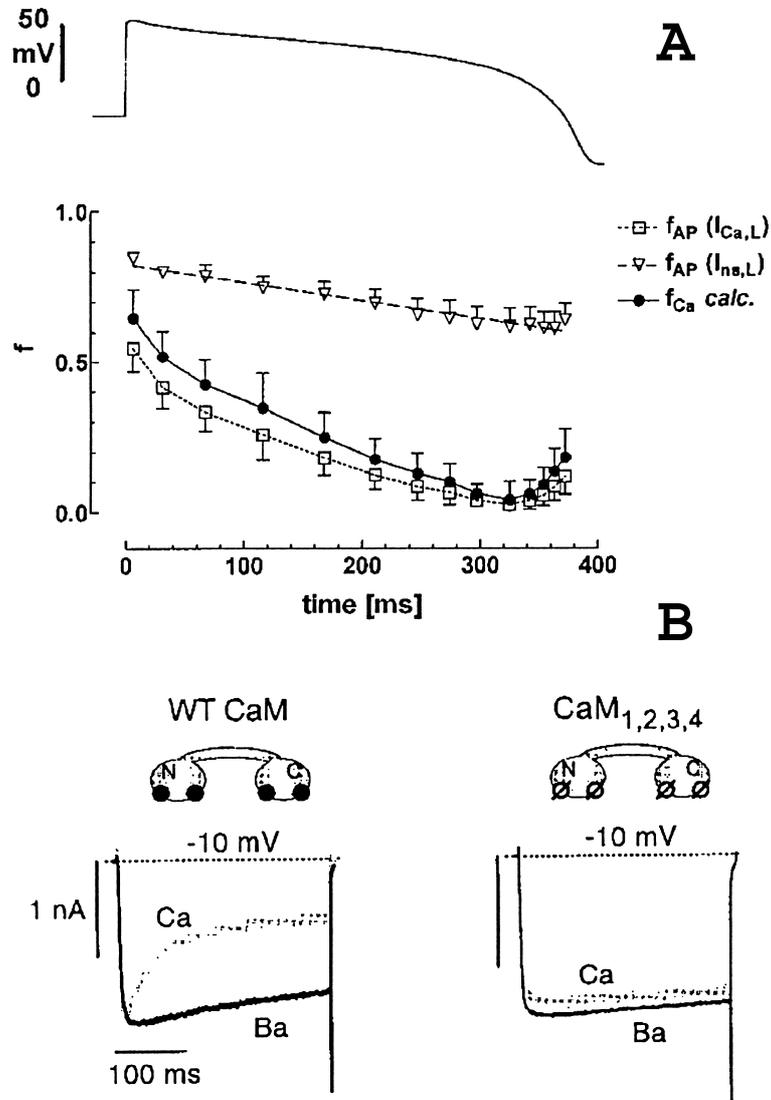
Fig. 3. (**A**) AP clamp waveform and estimates of the fraction of LCCs *not* voltage-inactivated (open triangles) and *not* Ca^{2+}-inactivated (*filled circles*) during the AP-clamp. Data measured in guinea pig ventricular myocytes. Reproduced from Fig. 11A–B of Linz and Meyer [12], with permission. (**B**) L-Type Ca^{2+} currents recorded from wild-type (WT CaM) rat ventricular myocytes or myocytes overexpressing mutant CaM (CaM$_{1,2,3,4}$). Responses are to voltage-clamp steps from a holding potential of -80 to -10 mV in the presence of Ca^{2+} (*dotted line*) or Ba^{2+} (*solid line*) as the charge carrier. Reproduced from Fig. 2 of Peterson et al. [10], with permission

of the channel and dissociation of FKBP12.6 increases RyR open probability and Ca^{2+} sensitivity [13]. Evidence suggests that cardiac RyRs may be physically coupled and exhibit coordinated gating which is functionally ablated in the absence of FKBP12.6 [14]. Cardiac RyRs contain a PKA phosphorylation site at serine-2809. The effects of PKA-induced phosphorylation of the RyR remains controversial, with one group asserting that phosphorylation leads to dissociation of FKBP12.6 from the RyR [15], thus regulating coordinated gating and channel open probability, while another group asserts that it does not [16]. Ca^{2+}/calmodulin-dependent protein kinase II (CaMKII) also phosphorylates RyR at serine-2815, leading to increased channel open probability and increased Ca^{2+} sensitivity [17].

2.2.3 Calcium-Induced Calcium-Release

EC Coupling involves a close interplay between LCCs and RyRs within the dyadic space. During the initial depolarization stages of the AP, voltage-gated LCCs open, allowing the entry of Ca^{2+} into the dyad. As Ca^{2+} concentration in the dyad increases, Ca^{2+} binds to the RyR, increasing their open probability and leading to Ca^{2+} release from the JSR – a process called Ca^{2+}-induced Ca^{2+} release (CICR).

The phenomenon of CICR has been studied extensively. Experiments have shown two major properties of CICR: (1) graded Ca^{2+} release; and (2) voltage-dependent EC coupling gain. *Graded release* refers to the phenomenon originally observed by Fabiato and co-workers [18, 19, 20] that Ca^{2+} release from JSR is a smooth and continuous function of trigger Ca^{2+} entering the cell via LCCs. Figure 4 (adapted from Fig. 3 of Wier et al. [21]) shows experimentally measured properties of graded release. Figure 4A shows trigger flux of Ca^{2+} through LCCs (open circles, F_{ICa}) and release flux of Ca^{2+} through RyRs (filled circles, $F_{SR,rel}$) in response to a range of depolarizing voltage-clamp steps. Both are smooth continuous functions of step potential. Figure 4B shows normalized versions of the flux curves. The curve for RyR release flux is shifted in the hyperpolarizing direction with respect to that for LCC trigger flux. This occurs since at lower membrane potentials, single LCC currents are large and thus highly effective at triggering opening of RyR. At higher potentials, closer to the reversal potential for Ca^{2+}, open probability of LCCs is high, but single channel currents are small and thus less effective at triggering opening of the RyR. *EC coupling gain* is defined as the ratio of peak Ca^{2+} release flux through RyRs to the peak trigger flux through LCCs. There are more RyRs than LCCs in mammalian cardiac ventricular cells, with the RyR:LCC ratio varying from 8:1 in rat, 6:1 in humans to 4:1 in guinea pig [22]. The result is that a greater amount of Ca^{2+} is released from JSR via the RyR than enters the cell through LCCs, leading to high EC coupling gain. Figure 4C shows an example of the EC coupling gain function in rat ventricular myocytes. The voltage dependence of gain arises from the relative displacement of the RyR and LCC flux curves shown in Fig. 4B.
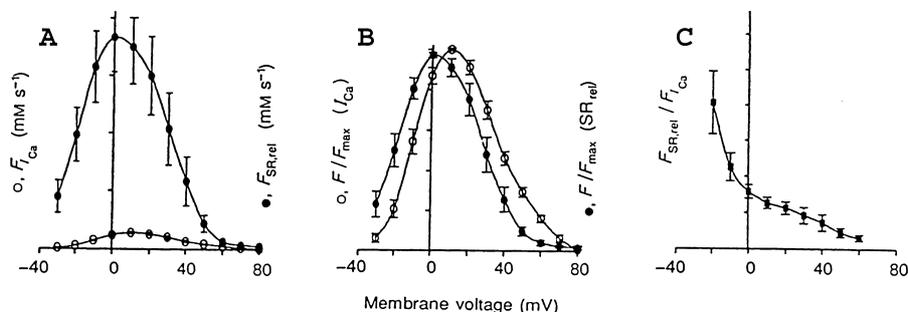
Fig. 4. (**A**) Ca^{2+} flux (ordinate, mM-s^{-1}) through RyRs (*filled circles*) and LCCs (*open circles*) as a function of membrane potential (abscissa, mV) measured from rat ventricular myoyctes. (**B**) Normalized data from Fig. 4A. (**C**) EC coupling gain (ordinate) as a function of membrane potential (abscissa, mV). Reproduced from Wier et al. [21] Fig. 3, with permission

2.2.4 Ca^{2+} Re-Uptake and Extrusion

Several mechanisms exist to restore Ca^{2+} concentration to resting levels following an AP (Fig. 2). These mechanisms are the Na^+-Ca^{2+} exchanger, the sarcolemmal Ca^{2+}-ATPase and the SR Ca^{2+}-ATPase [23]. The Na^+-Ca^{2+} exchanger is generally believed to import three Na^+ ions for every Ca^{2+} ion extruded, yielding a net charge movement [24]. More recent data support the idea that the exchange ratio may be 4:1 [25] or even variable [26]. The Na^+-Ca^{2+} exchanger is believed to be located predominantly in the sarcolemmal membrane and is driven by both transmembrane voltage and Na^+ and Ca^{2+} concentration gradients. It can work in forward mode, in which case it extrudes Ca^{2+} and imports Na^+, thus generating a net inward current, or in reverse mode, in which case it extrudes Na^+ and imports Ca^{2+} thus generating a net outward current. Some experimental evidence suggests that during the plateau phase of the AP, the Na^+-Ca^{2+} exchanger works initially in reverse mode bringing Ca^{2+} into the cell, and later switches to forward mode thereby extruding Ca^{2+} [27]. The second Ca^{2+} extrusion mechanism is the sarcolemmal Ca^{2+}-ATPase. This Ca^{2+} pump hydrolyzes ATP to transport Ca^{2+} out of the cell. It contributes a sarcolemmal current which is small relative to that of the Na^+-Ca^{2+} exchanger. At equilibrium, during each cardiac cycle (the time from the start of one AP to the next) the total amount of Ca^{2+} leaving the cell via the Na^+-Ca^{2+} exchanger and the sarcolemmal Ca^{2+}-ATPase is equal to the amount that enters. The third extrusion mechanism for myoplasmic Ca^{2+} is the SR Ca^{2+}-ATPase. This ATPase sequesters Ca^{2+} into the SR. The SR Ca^{2+}-ATPase is predominantly located in the NSR membrane. In equilibrium, during each cardiac cycle the SR Ca^{2+}-ATPase re-sequesters an amount of Ca^{2+} equal to that released by the SR via the RyR. The SR Ca^{2+}-ATPase hydrolyzes ATP to transport Ca^{2+}, and has both forward and

reverse modes [28, 29]. The reverse mode serves to prevent overloading of the SR with Ca^{2+} at rest.

3 Computational Models of Cardiac EC Coupling

3.1 Common Pool Models of CICR

In the majority of models of the cardiac ventricular myocyte, CICR is described either phenomenologically or through use of a formulation known as the "common pool" model. As defined by Stern [30] and as illustrated in Fig. 5, common pool models [31, 32, 33] are ones in which Ca^{2+} flux through all LCCs are lumped into a single trigger flux, Ca^{2+} flux through all RyRs is lumped into a single release flux and both the trigger and release flux are directed into a common Ca^{2+} compartment (labeled the "subspace" in Fig. 5). Consequently, in such models, activation of the JSR release mechanism is controlled by Ca^{2+} concentration in this common pool. The result of this physical arrangement is that once RyR Ca^{2+} release is initiated, the resulting increase of Ca^{2+} concentration in the common pool stimulates regenerative, all-or-none rather than graded Ca^{2+} release [30]. This "latch up" of Ca^{2+} release can be avoided and graded JSR release can be achieved in phenomenological models of EC coupling by formulating Ca^{2+} release flux as an explicit function of only sarcolemmal Ca^{2+} flux rather than as a function of Ca^{2+} concentration in the common pool [34, 35, 36, 37]. Models of this type are not common pool models based on the definition given by Stern, and do not suffer an inability to exhibit both high gain and graded JSR Ca^{2+} release. However, such phenomenological formulations lack mechanistic descriptions of the processes that are the
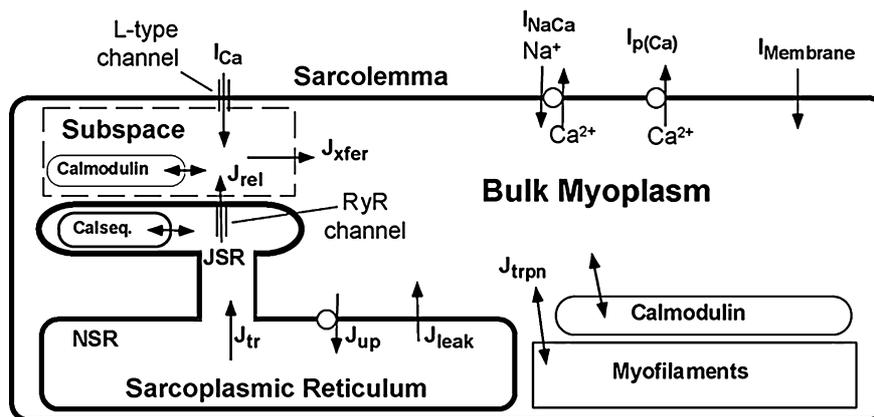

Fig. 5. Structure of a common pool myocyte model. Reproduced from Jafri et al. [31] Fig. 1, with permission

underlying basis of CICR. We therefore focus, in the remainder of this presentation, on a review of the strengths and weaknesses of the common pool model formulation.

3.1.1 Strengths of Common Pool Models

Despite the inability of common pool models to describe the fundamental property of graded JSR Ca^{2+} release, such models, when incorporated into integrative models of the myocyte, have proven reconstructive and predictive abilities. As will be discussed subsequently (Sect. 4.1), myocyte models based on the common pool formulation have been able to reconstruct many aspects of the cellular phenotype of ventricular myocytes isolated from end-stage failing canine and human hearts including prolongation of AP duration, reduced amplitude of intracellular Ca^{2+} transients and slowed decay of the Ca^{2+} transient (see Fig. 1 of Winslow et al. [32]). A common pool model of the guinea pig left ventricular myocyte has been able to reconstruct properties of extrasystolic restitution and post-extrasystolic potentiation in response to so-called S1-S2 stimulus protocols (see Fig. 5B of Rice et al. [38]). A recent computational model of the human left ventricular myocyte is able to predict rate-dependent prolongation of AP duration, AP duration restitution curves and Ca^{2+}-frequency relationships (see Figs. 5A, 6A and 7C of Iyer et al., respectively [39]). Thus, such models are able to account for a broad range of responses measured experimentally.

3.1.2 Weaknesses of Common Pool Models

In light of the successes detailed above, one may question whether graded JSR Ca^{2+} release plays an important role in shaping the electrophysiological responses of the ventricular myocyte. The answer is a definite "yes" and the reason has to do with recent data concerning the relative contribution of Ca^{2+}- versus voltage-dependent inactivation of LCCs reviewed in Sect. 2.2.1 and shown in Fig. 3. These data demonstrate that LCC Ca^{2+}-dependent inactivation is strong with rapid onset, whereas voltage-dependent inactivation is weaker with slower onset. In contrast, Fig. 6 shows the relationship between Ca^{2+}- and voltage-dependent LCC inactivation in three different models of the cardiac AP. Figures 6A–B replicate the experimental data of Linz and Meyer [12] and Figs. 6C–E show APs and Ca^{2+}- versus voltage-dependent inactivation of LCCs during these APs for common pool canine [32] and guinea pig [31] myocyte models and the Luo-Rudy guinea pig model incorporating a phenomenological description of CICR [36]. For each model, Ca^{2+} inactivation of LCCs is smaller or comparable in magnitude to voltage-dependent inactivation. This stands in contrast to the experimental data shown in Fig. 3.

   The consequence of incorporating the relationship between Ca^{2+}- versus voltage-dependent inactivation shown in Fig. 3 into a common pool model
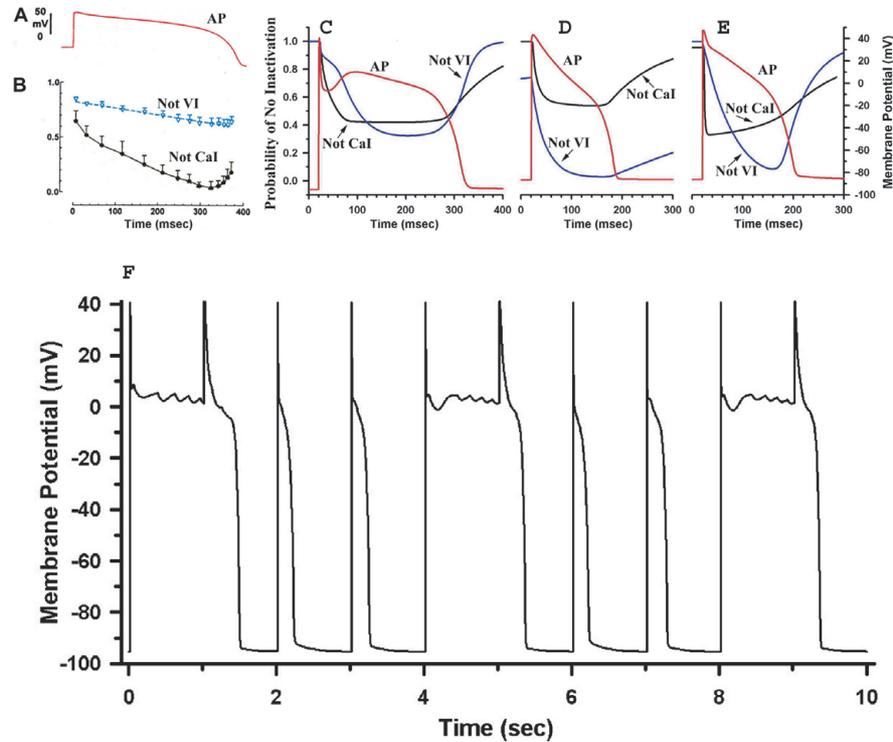
Fig. 6. Action potentials, fraction of LCCs not Ca^{2+}-inactivated (Not CaI) and not voltage-inactivated (Not VI) during the AP. (**A**) AP-clamp waveform used to control membrane potential of myocytes isolated from guinea pig left ventricle. (**B**) Experimental estimates of the fraction of LCCs not Ca^{2+}-inactivated and not voltage-inactivated when membrane potential is clamped as shown in Panel A. Panels C-E show similar estimates based on simulated actions potentials. Results are shown for APs generated using the Winslow et al. [32] (**C** – canine), Jafri-Rice-Winslow [31] (**D** – guinea pig), and Luo-Rudy Phase II [36] (**E** – guinea pig) ventricular myocyte models. **F**) Membrane potential as a function of time for a 10-second simulation of a modified version of the Winslow et al. [32] model with I_{CaL} parameterized with strongly Ca^{2+}-dependent and weakly voltage-dependent inactivation (similar to that of the local control model). Panels A and B are reproduced from Fig. 11 of Linz and Meyer [12], with permission

of the canine ventricular myocyte [32] is shown in Fig. 6F. AP duration becomes unstable. The reason for this is that in a model where the release of JSR Ca^{2+} is controlled by sensing Ca^{2+} levels in the same pool into which Ca^{2+} is released, Ca^{2+} release occurs in an all-or-none fashion [30]. When Ca^{2+}-dependent inactivation of LCCs is the dominant inactivation process in such common pool models, LCC inactivation also exhibits all-or-none behavior, switching on in response to JSR Ca^{2+} release and switching off in

its absence. This switching between all-or-none LCC inactivation destabilizes the plateau phase of the AP, with APs alternating between those with short ($\sim$150–250 ms) and long ($>$1000 ms) duration. This unstable behavior occurs over a wide range of LCC inactivation parameters as long as voltage-dependent inactivation of LCCs is relatively slow and weak. Strong voltage-dependent inactivation of I_{CaL}, although contrary to experimental observations, is therefore necessary to enforce stability of common pool models. When new data regarding the balance between voltage- and Ca^{2+}-dependent inactivation is incorporated into these models, they fail at reproducing even the most elementary electrophysiological response of the ventricular myocyte – a stable AP.

3.2 A Stochastic Local-Control Model of CICR

The fundamental failure of common pool models described above suggests that more biophysically-based models of EC coupling must be developed and investigated. Understanding of the mechanisms by which Ca^{2+} influx via LCCs triggers Ca^{2+} release from the JSR has advanced tremendously with the development of experimental techniques for simultaneous measurement of LCC currents and Ca^{2+} transients and detection of local Ca^{2+} transients and this has given rise to the local control hypothesis of EC coupling [21, 30, 40, 41]. This hypothesis asserts that opening of an individual LCC in the T-tubular membrane triggers Ca^{2+}-release from the small cluster of RyRs located in the closely apposed ($\sim$10 nm) JSR membrane. Thus, the local control hypothesis asserts that release is all-or-none at the level of these individual groupings of LCCs and RyRs. However, LCC and RyR clusters are physically separated at the ends of the sarcomeres [42]. These clusters therefore function in an approximately independent fashion. The local control hypothesis asserts that graded control of JSR Ca^{2+} release, in which Ca^{2+}-release from JSR is a smooth, continuous function of Ca^{2+} influx through LCCs, is achieved by the statistical recruitment of elementary Ca^{2+} release events in these independent dyadic spaces. Thus, at the heart of the local-control hypothesis is the assertion that the co-localization of LCCs and RyRs is a structural component that is fundamental to the property of graded Ca^{2+} release and force generation at the level of the cell.

Several computational models have been developed to investigate properties of local Ca^{2+} release at the level of the cardiac dyad [5, 43, 44, 45]. Each of these model formulations incorporates: (1) one or a few LCCs; (2) a cluster of RyRs; (3) the dyadic volume in which the events of CICR occur; and (4) anionic binding sites which buffer Ca^{2+}. In some of these models, detailed descriptions of diffusion and Ca^{2+} binding in the dyadic cleft are employed to demonstrate the effects of geometry, LCC and RyR properties and organization, and surface charge on the spatio-temporal profile of Ca^{2+} within the dyad, and hence on the efficiency of CICR [5, 44, 45]. Stern et al. [46] have simulated CICR stochastically using numerous RyR schemes to demonstrate

conditions necessary for stability of EC coupling and have suggested a possible role for allosteric interactions between RyRs. The functional release unit model of Rice et al. [43] has demonstrated that local control of CICR can be obtained without including computationally intensive descriptions of Ca^{2+} gradients within the dyadic space. Isolated EC coupling models such as these, however, cannot elucidate the nature of the interaction between local events of CICR and integrative cellular behavior, as the models are simply too computationally demanding.

We have recently developed a local-control model of CICR which is sufficiently minimal that it may be incorporated within a computational model of the cardiac ventricular myocyte [47]. This model is derived from a canine ventricular myocyte model [32] and incorporates stochastic gating of LCCs and RyRs. This model has been shown to capture fundamental properties of local control of CICR such as high gain, graded release and stable release termination. The model incorporates: (1) sarcolemmal ion currents of the Winslow et al. canine ventricular cell model [32]; (2) continuous time Markov chain models of the rapidly-activating delayed rectifier potassium current I_{Kr} [48], the Ca^{2+}-independent transient outward K current I_{to1} [49] and the Ca^{2+}-dependent transient outward chloride (Cl^-) current I_{to2}; (3) a continuous-time Markov chain model of I_{CaL} in which Ca^{2+}-mediated inactivation occurs via the mechanism of mode-switching [31]; (5) an RyR channel model adapted from that of Keizer and Smith [50]; and (6) locally controlled CICR from junctional sarcoplasmic reticulum (JSR) via inclusion of LCCs, RyRs, chloride channels, local JSR and dyadic subspace compartments within Ca^{2+} release units (CaRUs).

Figure 7 shows a schematic of the CaRU. The CaRU model is intended to mimic the properties of Ca^{2+} sparks in the T-tubule/SR (T-SR) junction. Figure 7B shows a cross-section of the model T-SR cleft, which is divided into four individual dyadic subspace compartments arranged on a 2×2 grid. Each subspace (SS) compartment contains a single LCC and 5 RyRs in its JSR and sarcolemmal membranes, respectively. All 20 RyRs in the CaRU communicate with a single local JSR volume. The 5:1 RyR to LCC stoichiometry is consistent with recent estimates indicating that a single LCC typically triggers the opening of 4–6 RyRs [51]. Each subspace is treated as a single compartment in which Ca^{2+} concentration is uniform, however Ca^{2+} may diffuse passively to neighboring subspaces within the same CaRU. The division of the CaRU into four subunits allows for the possibility that an LCC may trigger Ca^{2+} release in adjacent subspaces (i.e., RyR recruitment) under conditions where unitary LCC currents are large. The existence of communication among adjacent subspace volumes is supported by the findings that Ca^{2+} release sites can be coherent over distances larger than that occupied by a single release site [52], and that the mean amplitude of Ca^{2+} spikes (local SR Ca^{2+} release events that consist of one or a few Ca^{2+} sparks [53]), exhibits a bell shaped voltage dependence, indicating synchronization of multiple Ca^{2+} release events within
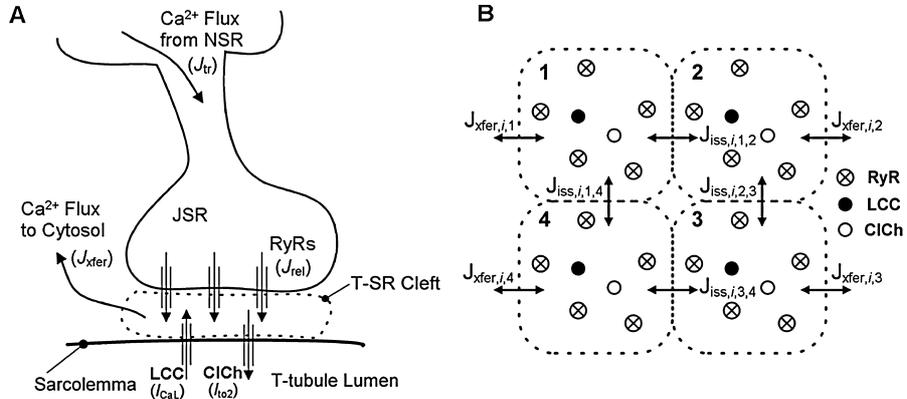
Fig. 7. Schematic representation of the Ca^{2+} release unit model (CaRU). (**A**) Trigger Ca^{2+} influx through the LCCs enters into the T-SR cleft (dyadic space). The rise in local Ca^{2+} level promotes the opening of RyRs and Ca^{2+}-modulated chloride channels (ClChs). The excess local Ca^{2+} passively diffuses out of the cleft into the cytosol and JSR Ca^{2+} is refilled via passive diffusion from the NSR. (**B**) The T-SR cleft (shown in cross-section) is composed of four dyadic subspace volumes, arranged on a 2×2 grid, each containing 1 LCC, 1 ClCh, and 5 RyRs. Ca^{2+} in any subspace may diffuse to a neighboring subspace (J_{iss}) or to the cytosol (J_{xfer}). $J_{iss,i,j,l}$ represents Ca^{2+} flux from the jth subspace to the lth subspace within the ith CaRU. Similarly $J_{xfer,i,j}$ represents Ca^{2+} flux from the jth subspace to the cytosol from the ith CaRU

a T-SR junction [54]. The choice of four subunits allows for semi-quantitative description of dyadic Ca^{2+} diffusion while limiting model complexity.

L-type Ca^{2+} current (I_{CaL}) is a function of the total number of channels (N_{LCC}), single channel current magnitude (i), open probability (p_o), and the fraction of channels that are available for activation (f_{active}), where $I_{CaL} = N_{LCC} \times f_{active} \times i \times p_o$. Single LCC parameters are based on experimental constraints on both i and p_o. The product $N_{LCC} \times f_{active}$ is chosen such that the amplitude of the whole-cell current agrees with that measured experimentally in canine myocytes. This approach yields a value of 50,000 for $N_{LCC} \times f_{active}$, consistent with experimental estimates of active LCC density and corresponding to 12,500 active CaRUs.

One of the bases for local control of SR Ca^{2+} release is the structural separation of T-SR clefts at the ends of sarcomeres (i.e., RyR clusters are physically separated) [42]. Each CaRU is therefore simulated independently in accord with this observation. Upon activation of RyRs, subspace Ca^{2+} concentration increases. This Ca^{2+} will diffuse freely to either adjacent subspace compartments (J_{iss}) or into the cytosol (J_{xfer}) as determined by local concentration gradients. The local JSR compartment is refilled via passive diffusion of Ca^{2+} from the network SR (NSR) compartment (J_{tr}).

The algorithm for solving the stochastic ordinary differential equations defining the model has been described previously [47]. Briefly, transition rates for each channel are determined by their gating schemes and their dependence on local Ca^{2+} level. Gating of each channel within a CaRU is simulated by choosing channel occupancy time as an exponentially distributed random variable with parameter determined by the sum of voltage- and/or Ca^{2+}-dependent transition rates from the current state. Stochastic simulation of CaRU dynamics is used to determine all Ca^{2+} flux into and out of each local subspace. The summation of all Ca^{2+} fluxes crossing the CaRU boundaries are taken as inputs to the global model, which is defined by a system of coupled ordinary differential equations. The dynamical equations defining the global model are solved using the Merson modified Runge-Kutta 4th-order adaptive time step algorithm which has been modified to embed the stochastic CaRU simulations within each time step.

This model provides the ability to investigate the ways in which LCC, RyR and subspace properties impact on CICR and the integrative behavior of the myocyte. However, this ability is achieved at a high computational cost. Three approaches are therefore used to accelerate the computations. First, the pseudo-random number generator used is the Mersenne Twister algorithm [55], having a long period ($2^{19937}-1$) and reduced computation time. Second, we have developed an algorithm for the dynamic allocation of model CaRUs so that a large number of CaRUs are utilized prior to, during and shortly after the AP, and a smaller number of CaRUs is used during diastole. Third, simulation of the stochastic dynamics of the independent functional units may be performed in parallel, resulting in near linear speedup as the number of processors is increased. These modifications enable us to simulate up to 1 Sec of model activity in 1 minute of simulation time when running on 6 IBM Power4 processors configured with 4 Gbytes memory each.

Figure 8 shows macroscopic properties of APs and SR Ca^{2+} release in this hybrid stochastic/ODE model. Figure 8A shows the voltage dependence of peak Ca^{2+} flux (ordinate) through LCCs (filled circles) and RyRs (open circles) as a function of membrane potential (mV, abscissa). Unlike the case for common pool models, Ca^{2+} release flux is a smooth and continuous function of membrane potential, and hence trigger Ca^{2+}, as shown by the experimental data in Fig. 4A. Figure 8B shows the data of Fig. 8A following normalization. The model data exhibit the hyperpolarizing shift of release flux relative to trigger flux seen in the experimental data of Fig. 4B. EC coupling gain (ordinate) is shown as a function of membrane potential (mV, abscissa) in Fig. 8C. Open boxes show gain when there is no Ca^{2+} diffusion between the 4 functional release units comprising each CaRU, and the open triangles show gain when such diffusion is accounted for. In the presence of Ca^{2+} diffusion between functional units comprising each CaRU, EC coupling gain is greater at all potentials, but the increase in gain is most dramatic at more negative potentials. In this negative voltage range, LCC open probability is sub-maximal, leading to sparse LCC openings. However, unitary current magnitude is
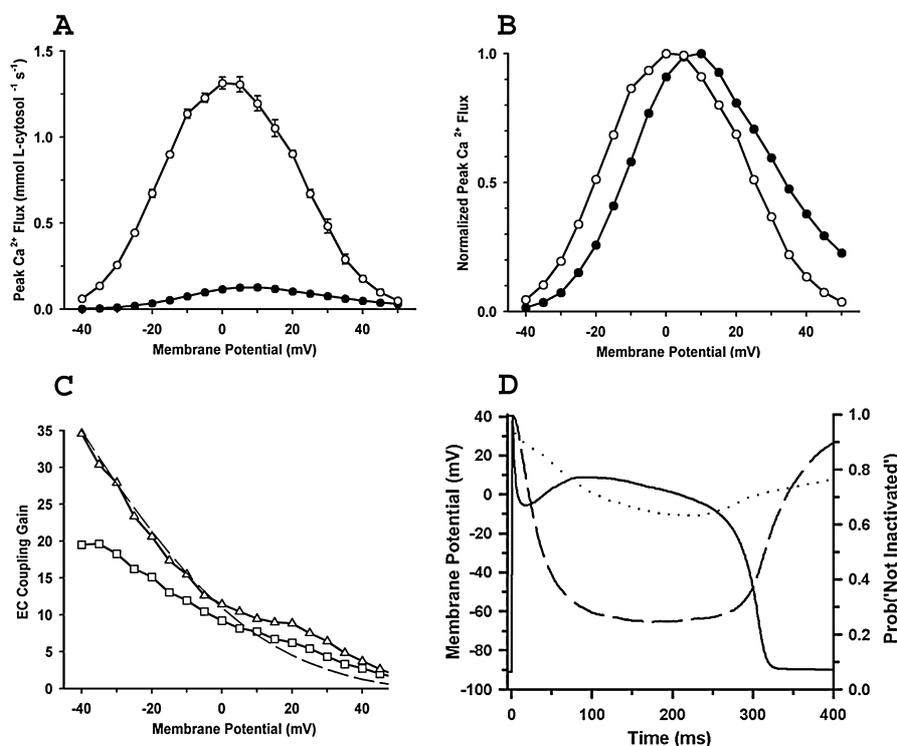
Fig. 8. Voltage dependence of macroscopic LCC Ca^{2+} influx, SR Ca^{2+} release, and EC coupling gain. (**A**) Mean peak Ca^{2+} flux amplitudes, $F_{\mathrm{LCC(max)}}$ (*filled circles*) and $F_{\mathrm{RyR(max)}}$ (*open circles*) as a function of membrane voltage, $n = 5$ simulations at each voltage. (**B**) Peak Ca^{2+} fluxes (data of panel A) normalized by their respective maxima. (**C**) EC coupling gain as a function of membrane potential defined as $F_{\mathrm{RyR(max)}}/F_{\mathrm{LCC(max)}}$ under control conditions (*triangles*) and in the absence of intersubspace coupling within the CaRUs (*squares*), as well as L-type unitary current (*dashed line*, scaled to match the gain function at –40 mV). (**D**) Action potential (*solid line*) obtained in the stochastic local control model incorporating the relationship between V- and Ca^{2+}-dependent inactivation measured by Linz & Meyer [12]

relatively high, so that in the presence of Ca^{2+} diffusion within the CaRU, the rise in local Ca^{2+} due to the triggering action of a single LCC can recruit and activate RyRs in adjacent subspace compartments within the same T-SR junction. The net effect of inter-subspace coupling is therefore to increase the magnitude and slope of the gain function preferentially in the negative voltage range.

Figure 8D shows the relative balance between the fraction of LCCs *not* voltage-inactivated (dotted line) and *not* Ca^{2+}-inactivated (dashed line) during an AP simulated using the local-control ventricular myoycte model. These fractions were designed to fit the experimental data of shown in Fig. 3A. The

solid line shows a local-control model AP. This AP should be contrasted with those produced by the common pool model (Fig. 6F) when the same relationship between LCC voltage- and Ca^{2+}-dependent inactivation is used. Clearly, the local-control model exhibits stable APs whereas the common pool model does not. These simulations therefore offer an intriguing glimpse of the functional importance of local control of CICR in shaping properties of the AP and of how co-localization and stochastic gating of individual channel complexes can have a profound effect on the integrative behavior of the myocyte.

3.3 Coupled LCC-RyR Gating Models of CICR

The results described above demonstrate that to accommodate new data regarding strong negative feedback regulation of LCC function by JSR Ca^{2+} release, myocyte models must incorporate graded CICR. Unfortunately, local control models based on stochastic simulation of CaRU dynamics remain far too computationally demanding to be used routinely by most laboratories in single cell simulations, let alone in models of cardiac tissue.

To address this problem, we have recently formulated a novel model of CICR which describes the underlying channels and local control of Ca^{2+} release, but consists of a low dimensional system of ordinary differential equations [56]. This is achieved in two steps, using the same techniques as applied by Hinch in an analysis of the generation of spontaneous sparks in a model of a cluster of RyRs [57]. First, the underlying channel and CaRU models are minimal, such that they only contain descriptions of the essential biophysical features observed in EC coupling. This in turn yields a system of model equations which can be simplified by applying approximations based on a separation of time-scales. In particular, it can be shown that Ca^{2+} in the dyadic space equilibrates rapidly relative to the gating dynamics of LCCs and RyRs. The joint behavior of LCCs and RyRs can then be described using a Markov model where the transition probabilities between interacting states are a function of global variables only. This in turn allows the ensemble behavior of the CaRUs to be calculated using ordinary differential equations. The resulting model, which we refer to as the coupled LCC-RyR gating model, has parameters which may be calculated directly from the underlying biophysical model of local control of Ca^{2+} release. Despite the simplicity of this model, it captures key properties of CICR including graded release and voltage-dependence of EC coupling gain. The model is therefore well suited for incorporation within single cell and tissue models of ventricular myocardium.

3.3.1 A "Minimal" Coupled LCC-RyR Gating Model

The model of local-control of CICR which we will develop is minimal in the sense that: (a) CaRUs consist of only one LCC, one RyR and the subspace within which they communicate; and (b) simplified continuous time Markov models of LCC and RyR gating are employed, each consisting of three-states.

Despite this simplicity, the model is able to describe key properties of local-control of CICR. The following sections provide a brief overview of model development. Full details are given in Hinch et al. [57].

As a starting point for development of a minimal LCC model, we use the LCC model developed by Jafri et al. [31] and modified by Greenstein and Winslow [47]. This model was formulated based on the molecular structure of the channel which is assumed to be composed of four independently gating subunits [31]. This leads to an activation process described by five closed states. The model is shown in Fig. 9A. LCCs are assumed to gate in a "Mode Normal" in which they are not Ca^{2+}-inactivated, and a "Mode Ca" in which they are Ca^{2+}-inactivated. Horizontal transitions in either mode are voltage-dependent, with rightward transitions corresponding to channel activation following membrane depolarization. In Mode Normal, the final transition from state C_4 to the open conducting state O is voltage-independent. In Mode Ca, transitions from IC_4 to an open state do not exist, corresponding to channel inactivation. Vertical transitions are voltage-independent, with transition rates from Mode Normal to Mode Ca being a function of Ca^{2+} concentration in the dyadic space, denoted as $[Ca^{2+}]_{ds}$.

The model is first simplified by reducing the number of closed and closed-inactivated states. The resulting model is shown in Fig. 9B. The model consist of two closed states (denoted C_3 and C_4), a single open state O accessible from closed state C_4 and two Ca^{2+}-inactivated states IC_3 and IC_4. While the structure of this reduced 5-state model is no longer based on the molecular structure of the LCC, it retains the essential functional features of the full model such as well-defined gating modes and rates of Ca^{2+}-mediated inactivation which depend upon activation (rightward transitions) of the channel. This model can be simplified further to a 3-state model (Fig. 9C) by using the fact that transitions between the state pairs C_3 and C_4 and IC_3 and IC_4 are rapid relative to the transition rates between these two sets of states. Define the combined closed state $C = C_3 \cup C_4$ and the combined inactivated state $I = IC_3 \cup IC_4$. Since the time-scale of the transitions between C_3 and C_4 is the smallest time-scale in the model, we can assume that these 2 states are in equilibrium and thus define conditional state occupancy probabilities as

$$P(C_3/C) = \frac{a_{-1}}{a_{-1} + a_1}$$

$$P(C_4/C) = \frac{a_1}{a_1 + a_{-1}}$$

A similar approximation is applied to states IC_3 and IC_4. Under these assumptions, the forward transition rate between the combined closed state C and the combined inactivated state I is given by

$$\varepsilon_+([Ca^{2+}]_{ds}) = a\varepsilon_1([Ca^{2+}]_{ds})P(C_3|C) + \varepsilon_1([Ca^{2+}]_{ds})P(C_4|C)$$

A similar approach may be used to derive the remaining transition rates between states I, C and O. The open channel current is then given by the
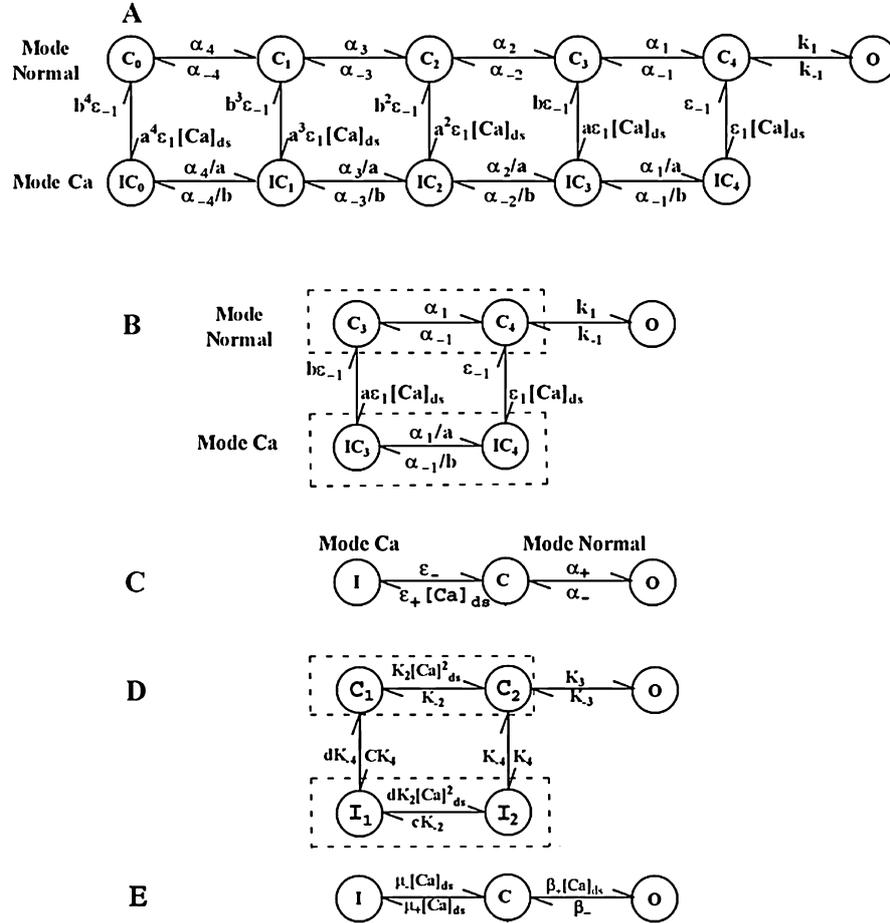
Fig. 9. (**A**) The 11-state LCC model developed by Jafri et al. [31]. (**B**) Simplification of the model in (**A**) by truncation of the leftmost 3 columns of states. (**C**) Simplification of the model in (**B**) by applying the rapid equilibrium approximation to state pairs C_3 and C_4 and IC_3 and IC_4. (**D**) 5-state RyR model from Stern et al. [46]. (**E**) Simplification of the 5-state model in (**D**) by application of the rapid equilibrium approximation to state pairs C_1 and C_2 and I_1 and I_2

Goldman-Hodgkin-Katz equation (see Hinch et al. [56]). This model of the LCC will be validated against experimental data in the following section.

We use a 5-state model of the RyR (Fig. 9D) based on Scheme 6 of Stern et al. [46], with the addition of modal gating between states C and O. Transitions from the closed to open modes occur upon binding of two Ca^{2+} ions. Transitions between states C_1 and C_2, and inactivated states I_1 and I_2 are assumed to be rapid. Following the same procedure used in the reduction of the LCC model, the RyR model is reduced to a 3-state model (Fig. 9E).

The magnitude of the Ca^{2+} flux through an open RyR is proportional to the difference in Ca^{2+} concentration between the SR and the local dyadic space.

We employ a minimal model for each CaRU consisting of one LCC, one RyR and the dyadic space within which these channels reside. Experimental recordings of triggered Ca^{2+}-sparks show that a single LCC opening may activate 4–6 RyRs [51]. The CaRU model employed here is therefore a simplification of actual dyadic structure and function as described previously. Several prior models of CaRUs [47, 58] also include a local JSR volume which is depleted relative to the network SR during Ca^{2+} release. However, recent experimental studies suggest that the JSR Ca^{2+} is in quasi-equilibrium with network SR during Ca^{2+} release [59]. Therefore, the minimal CaRU model does not include a local JSR. Calcium flux from the dyadic space to the cytoplasm is governed by simple diffusion, such that the time-evolution of $[Ca^{2+}]_{ds}$ is given by

$$V_{ds}\frac{d[Ca^{2+}]_{ds}}{dt} = J_{RyR} + J_{LCC} - g_D([Ca^{2+}]_{ds} - [Ca^{2+}]_i)$$

where V_{ds} is the volume of the dyadic space, $[Ca^{2+}]_i$ is the Ca^{2+} concentration in the myoplasm, g_D is the conductance, and J_{RyR} and J_{LCC} are the currents through the RyR and LCC, respectively. The time constant of equilibrium of $[Ca^{2+}]_{ds}$, is given by $\tau_{ds} = V_{ds}/g_D \approx 3\,\mu s$ [57, 58]. Since this time constant is considerably smaller than that for opening of either LCC or RyR channels, we may use the rapid equilibrium approximation [57] to show that

$$[Ca^{2+}]_{ds} \sim [Ca^{2+}]_i + \frac{J_{RyR} + J_{LCC}}{g_D}$$

This is *the crucial step* in model simplification since $[Ca^{2+}]_{ds}$ is now a function of only the global variables $[Ca^{2+}]_{SR}$, $[Ca^{2+}]_i$, V and the state of the local RyR and LCC. As a result of this simplification, it is no longer necessary to solve a differential equation for each $[Ca^{2+}]_{ds}$ when modeling all CaRUs in the myocyte. Rather, $[Ca^{2+}]_{ds}$ is an algebraic function of the fluxes into and out of the dyadic space.

Armed with this simplification, it is now possible to define a state model in which each state describes the joint behavior of the LCC and RyR in each CaRU. Define Y_{ij} (where $i, j =$ C, O, I) as the state of the CaRU with the LCC in the ith state and the RyR in the jth state. The CaRU can then be in one of 9 macroscopic states (Fig. 10). $[Ca]_{ds}$, J_{RyR} and J_{LCC} must be calculated separately for each of the 9 states. For example, consider the state Y_{co} with the LCC closed ($J_{LCC} = 0$) and the RyR open ($J_{RyR} = J_R\left([Ca^{2+}]_{SR} - [Ca^{2+}]_{ds}\right)$), then the rapid equilibrium approximation yields

$$c_{CO} = \frac{[Ca^{2+}]_i + \frac{J_R}{g_D}[Ca^{2+}]_{SR}}{1 + \frac{J_R}{g_D}}$$

$$J_{R,CO} = J_R \frac{[\mathrm{Ca}^{2+}]_{\mathrm{SR}} - [\mathrm{Ca}^{2+}]_i}{1 + \frac{J_R}{g_D}}$$

where $[\mathrm{Ca}^{2+}]_{\mathrm{ds}}^{\mathrm{co}}$ is $[\mathrm{Ca}^{2+}]_{\mathrm{ds}}$ in the state Y_{co} and $J_{\mathrm{RyR}}^{\mathrm{co}}$ is J_{RyR} in the state Y_{co}. Results for other states may be derived similarly. The resulting 9 state model of the CaRU shown in Fig. 10 is what we refer to as the coupled LCC-RyR gating model. Note that transitions are a function of $[\mathrm{Ca}^{2+}]_{\mathrm{ds}}$ which is itself a function of model states.
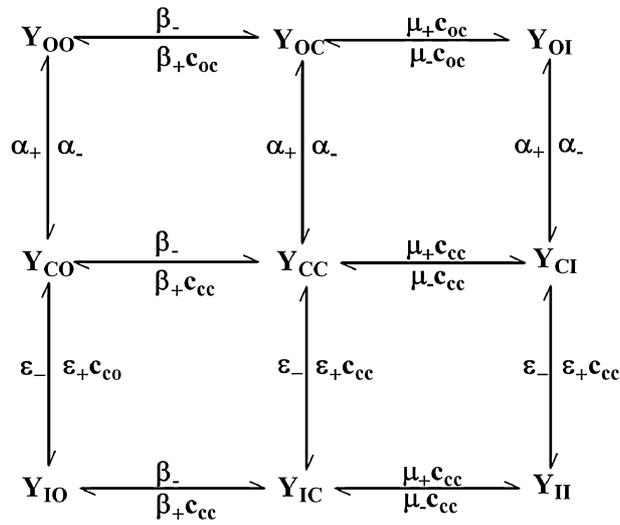

Fig. 10. The minimal coupled LCC-RyR gating model. States Y_{ij} denote the fraction of CaRUs in which the LCC is in state i and the RyR is in state j

The laws of mass action may next be used to derive a system of (eight) differential equations describing the time evolution of the fraction of LCC-RyR channels occupying the various states shown in Fig. 10. Whole cell Ca^{2+} currents are calculated by summing the contributions from the populations of CaRUs for which at least one LCC or RyR is open.

Figure 11A shows normalized peak flux through LCCs and RyRs (ordinate) as a function of membrane potential. As described previously, Ca^{2+} release is most effective at those membrane potentials producing large single LCC currents [21]. This results in the peak of the normalized JSR Ca^{2+} release flux being shifted by about $10\,\mathrm{mV}$ in the hyperpolarizing direction relative to the peak of the LCC trigger flux, as shown in the experimental data of Fig. 4B and in results from the stochastic local control model of Fig. 8B. This important behavior is also captured by the coupled LCC-RyR gating. As a consequence of this relative displacement of peak values, EC coupling gain decreases with increasing membrane potential. Figure 11B shows EC coupling
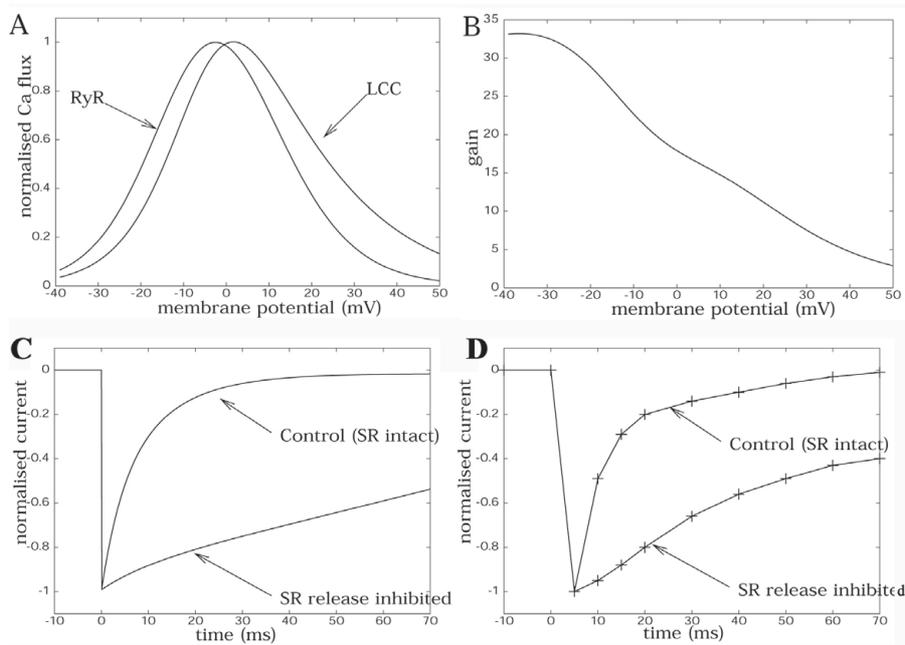
Fig. 11. (**A**) Normalized peak LCC and RyR flux (ordinate) as a function of membrane potential (abscissa, mV) for the minimal coupled LCC-RyR gating model. (**B**) EC coupling gain (ordinate) as a function of membrane potential (abscissa, mV) for the minimal coupled LCC-RyR gating model. Time course of LCC current after a voltage step from $-50\,\mathrm{mV}$ to $+10\,\mathrm{mV}$ for the minimal LCC-RyR coupled gating model (**C**) versus that measured experimentally in rat ventricular myocytes (**D**) [60]

gain (ordinate) as a function of membrane potential (abscissa, mV) predicted using the coupled LCC-RyR gating model. Results are in good agreement with both experimental data (Fig. 4C) and the stochastic local control model (Fig. 8C), thus demonstrating that despite its simplicity, the coupled LCC-RyR gating model is able to reconstruct the most critical feature of local control of CICR.

In voltage-clamp experiments in which JSR Ca^{2+} release is intact, it is found that the L-Type Ca^{2+} current is inactivated after approximately 20 ms. However, when JSR Ca^{2+} is depleted by application of caffeine, ryanodine or application of pre-pulses, Ca^{2+} inactivation is much slower. Figure 11C shows a comparison of the model prediction of this effect with experimental results (Fig. 11D) obtained in voltage-clamp studies using ventricular myocytes isolated from rat heart [60]. In both model and experiment, the cell was clamped at $-50\,\mathrm{mV}$ and then stepped to $10\,\mathrm{mV}$ for $70\,\mathrm{ms}$. JSR Ca^{2+} was depleted in the model by setting it to 10% of its normal value. Experimental and model results are in close agreement.

3.3.2 Generalized Coupled LCC-RyR Gating Models

The minimal nature of the model described above places some limits on its suitability for EC coupling and whole myocyte simulation studies. Such a model will be appropriate for large scale, multi-cellular simulations, but may be insufficient to quantitatively predict more complex cellular dynamics which depend upon the details of CICR. The method described above for deriving a coupled LCC-RyR, however, is not limited only to such highly reduced minimal models. We have developed a technique to build a coupled LCC-RyR gating model based on a CaRU which may contain one or more LCCs and/or RyRs, and where the individual channel models may maintain a greater level of complexity. Manual derivation of the equations describing such models would be an inefficient and error prone process because increased complexity and/or number of individual channel models leads to rapid growth in the number of equations required to describe the coupled system. For example, a CaRU with one 10-state LCC and five 4-state RyRs (see Fig. 12) will become a coupled LCC-RyR model consisting of 560 states. We have therefore designed and implemented an algorithm which generates the full set of model equations based on the number, structure and parameters supplied for the individual LCC and RyR models. As described above, rapid equilibrium for Ca^{2+} flux in the dyadic space is applied to determine the $[Ca^{2+}]_{ds}$ for each possible LCC-RyR open-closed combination as an algebraic function of only the global variables $[Ca^{2+}]_{SR}$, $[Ca^{2+}]_i$, and V. A general CaRU model consisting of N_{LCC} M_{LCC}-state LCCs and $N_{RyR}M_{RyR}$-state RyRs can therefore be employed.

The minimal coupled LCC-RyR model was derived using an LCC model which does not contain a voltage-dependent inactivation mechanism. As described above, the appropriate balance between voltage- and Ca^{2+}-dependent inactivation of the L-type Ca^{2+} current can only be achieved at present in a local control myocyte model (Fig. 8D). Here we develop a coupled LCC-RyR model which retains these properties of LCC inactivation and can be used as a replacement for the computationally expensive stochastic simulation of locally controlled CICR in the canine myocyte model described earlier. The LCC model consists of five states in the same configuration as those of Fig 9B. These represent the channel when it is not voltage-inactivated. In addition, each of the five states has an analogous voltage-inactivated state, where the voltage dependence of inactivation is that used previously in the stochastic local control model [47]. All voltage-inactivated states are closed states. The result is a 10-state LCC model which incorporates separate mechanisms of voltage- and Ca^{2+}-dependent inactivation. The RyR is modeled with the 4-state model used previously in the canine myocyte [47]. It is assumed that the baseline model contains only one LCC and one RyR per CaRU, yielding a 40-state coupled LCC-RyR model.

Figure 12 shows EC coupling gain (ordinate) as a function of membrane potential (mV, abscissa) for the baseline model (short dashed line). The gain
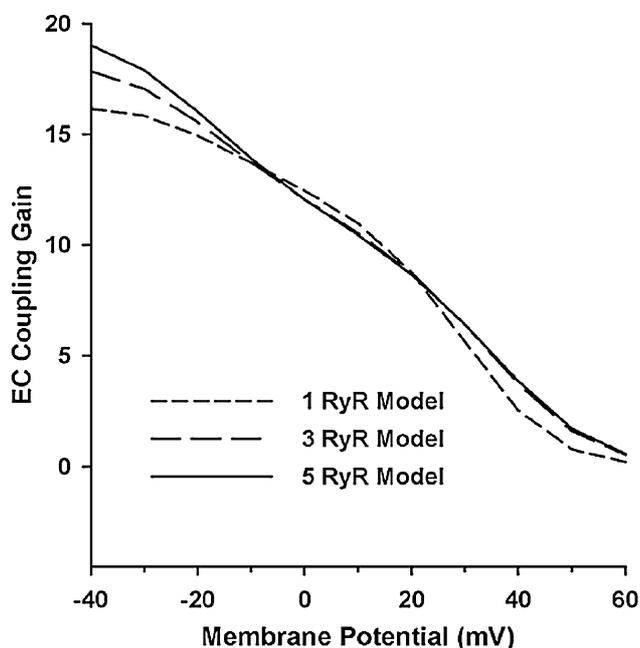
Fig. 12. EC coupling gain as a function of membrane potential (mV) for coupled LCC-RyR models consisting of 1 RyR (*short dashed line*), 3 RyRs (*long dashed line*), and 5 RyRs (*solid line*)

function decreases with increasing potential similar to that shown for the stochastic local control model (Fig. 8C). Since single LCC openings have been shown to activate 4-6 RyRs [51], the inclusion of only one RyR is a model reducing simplification. To test the validity of this model reduction, Fig. 12 also shows EC coupling gain for models which include 3 RyRs per CaRU (long dashed line) and 5 RyRs per CaRU (solid line). The 3-RyR model yields a 200-state coupled LCC-RyR model and the 5-RyR model yields a 560-state coupled LCC-RyR model. Parameters of each model were adjusted such that all models generated nearly identical APs (with duration of ∼300 ms at 1 Hz pacing interval) and such that the total open channel Ca^{2+} flux summed over all RyRs in a CaRU was conserved. The results demonstrate that under these conditions there is little variation in EC coupling gain as a function of the number RyRs in the CaRU and therefore justify the choice of one RyR per CaRU for the baseline model. These findings are consistent with experiments that have indicated that RyRs are functionally coupled and may gate synchronously [14].

Figure 13 demonstrates the ability of the baseline coupled LCC-RyR model, when incorporated into the whole cell model of Greenstein and Winslow [47], to reconstruct action potentials and Ca^{2+} transients of normal
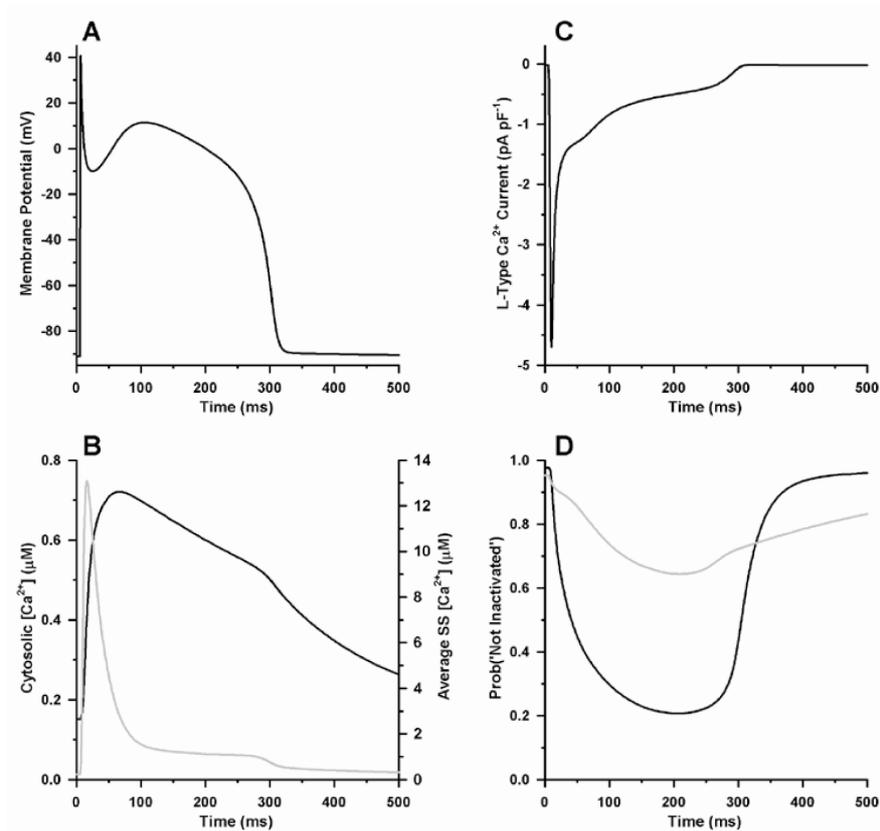
Fig. 13. Whole cell properties of the local control canine myocyte model employing the baseline (1 RyR) coupled LCC-RyR model of CICR. Signals shown are in response to a 1-Hz pulse train, with responses shown in steady-state. (**A**) Action potential simulated under normal conditions. (**B**) Cytosolic (*black line, left axis*) and mean subspace (*gray line, Right axis*) Ca^{2+} concentrations corresponding to the AP simulated in panel A. (**C**) L-type Ca^{2+} current (I_{CaL}) corresponding to the AP simulated in panel A. (**D**) Fraction of LCCs not Ca^{2+}-inactivated (*black line*) and not voltage-inactivated (*gray line*) underlying I_{CaL} (panel C for the AP simulated in panel A

canine midmyocardial ventricular myocytes. In Fig. 13A a normal 1-Hz steady-state AP is shown, and has similar shape and duration ($\sim$300 ms) to that of the stochastic model of Fig. 8D [47]. Figure 13B shows cytosolic (black line) and mean subspace (gray line) Ca^{2+} transients. While the cytosolic Ca^{2+} transient peaks at $\sim$0.75 μm, and lasts longer than the duration of the AP, Ca^{2+} in the subspace reaches $\sim$13 μm on average, and equilibrates to near cytosolic levels rapidly within $\sim$100 ms, similar to that observed in the stochastic local control model [47]. L-type current during the AP is shown in Fig. 13C, and

peaks at $\sim$4.7 pA pF^{-1} with a sustained component of $\sim$0.5$-$0.7 pA pF^{-1} which lasts for nearly the entire duration of the AP. Figure 13D shows the relative balance between the fraction of LCCs *not* voltage-inactivated (gray line) and *not* Ca^{2+}-inactivated (black line) during an AP. These fractions agree with the experimental data of shown in Fig. 3A, and the stochastic local control model simulations of Fig. 8D. These results demonstrate that the salient features of the AP, Ca^{2+} cycling, and the balance of voltage- and Ca^{2+}-mediated inactivation of LCCs can be adequately captured in a local control model which employs a relatively low order (40-state), and therefore highly efficient, coupled LCC-RyR model.

4 Modeling Applications

4.1 AP Duration Regulation in Heart Failure

Heart failure (HF), the most common cardiovascular disorder, is characterized by ventricular dilatation, decreased myocardial contractility and cardiac output. Prevalence in the general population is over 4.5 million, and increases with age group to levels as high as 10%. New cases number approximately 400,000 per year. Patient prognosis is poor, with mortality roughly 15% at one year, increasing to 80% at six years subsequent to diagnosis. It is now the leading cause of Sudden Cardiac Death (SCD) in the U.S., accounting for nearly half of all such deaths.

Failing myocytes exhibit altered patterns of expression of several genes/ proteins involved in shaping the cardiac AP. These changes of expression result in prolongation of AP duration (see experimental data in Fig. 14A) and reduction of Ca^{2+} transient amplitude (see experimental data of Fig. 14B). The molecular basis of these changes is now known. Measurements of whole-cell inward rectifier current I_{K1} show that current density at hyperpolarized membrane potentials is reduced in HF by $\sim$50% in human [61], and by $\sim$40% in dog [62]. Measurements of I_{to1} show that in end-stage HF human and canine tachycardia pacing-induced HF indicate current density is reduced by up to 70% in HF [61, 62, 63]. No change was observed in either voltage-dependence or kinetics of the I_{to1} current, only a reduction of channel density. Expression of diverse proteins involved in the processes of EC coupling has also been measured in normal and failing myocytes. These proteins include the SR Ca^{2+}-ATPase encoded by the SERCA2α gene and the sodium-calcium (Na^{+}-Ca^{2+}) exchanger protein encoded by the NCX1 gene. Measurements indicate there is an approximate 50% reduction of SERCA2α mRNA, expressed protein level and direct SR Ca^{2+}-ATPase uptake rate in end-stage HF [64]. There is a 55% increase in NCX1 mRNA levels, and an approximate factor of two increase in Na^{+}-Ca^{2+} exchange activity in end-stage HF [64].

In previous work, we investigated the mechanisms by which AP duration is prolonged in ventricular myocytes isolated from failing end-stage hearts
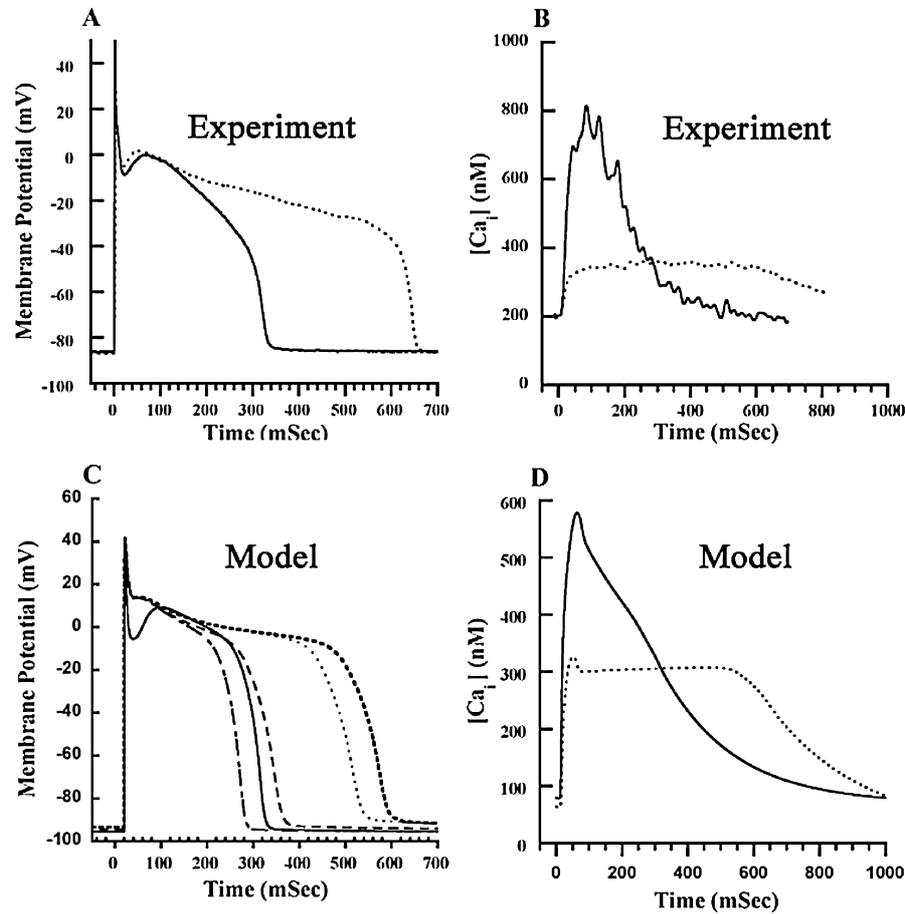
Fig. 14. Model versus experimental action potentials and Ca^{2+} transients. Each action potential and Ca^{2+} transient is in response to a 1 Hz pulse train, with responses measured in the steady-state. (**A**) Experimentally measured membrane potential (mV – ordinate) as a function of time (mSec – abscissa) in normal (*solid*) and failing (*dotted*) canine myocytes. (**B**) Experimentally measured cytosolic Ca^{2+} concentration (nmol/L – ordinate) as a function of time (mSec – abscissa) for normal (*solid*) and failing (*dotted*) canine ventricular myocytes. (**C**) Membrane potential (mV – ordinate) as a function of time (mSec – abscissa) simulated using the normal canine myocyte model (*solid*), and with the successive down-regulation of I_{to1} (*dot-dashed*, 66% down-regulation), I_{K1} (*long-dashed* – down-regulation by 32%), SERCA2α (rightmost *short-dashed* – down-regulation by 62%) and NCX1 (*dotted* – up-regulation by 75%). (**D**) Cytosolic Ca^{2+} concentration (nmol/L – ordinate) as a function of time (mSec – abscissa) simulated using the normal (*solid*) and heart failure (*dotted*) model. Reproduced from Fig. 1 of Winslow et al. [32], with permission

[32, 65]. To do so, we formulated a minimal model of altered repolarization and Ca^{2+} handling in ventricular cells from the failing canine heart incorporating: (a) reduced expression of I_{K1} and I_{to1}; (b) down-regulation of the SR Ca^{2+}-ATPase; and (c) up-regulation of the Na^{+}-Ca^{2+} exchanger. Figures 14C–D demonstrate the ability of the model to reconstruct APs and Ca^{2+} transients measured in both normal and failing canine midmyocardial ventricular myocytes. Figure 14C shows a normal model AP (solid line), and model APs corresponding to the additive effects of sequential down-regulation of I_{to1} (by 62%; dot-dashed line), I_{K1} (by 32%; long-dashed line), and SERCA2α (by 62%; rightmost short-dashed bold line), followed by up-regulation of NCX1 (by 75%; dotted line). Down-regulation of I_{to1} produces a modest *shortening* of AP duration. On first consideration, this seems an anomalous effect, but is one which agrees with recent experiments in canine. The model predicts the mechanism of AP duration shortening is a reduction in driving force due to reduction of the Phase I notch and a reduction in delayed activation of $I_{Ca,L}$ [49]. The additional down-regulation of I_{K1} (long-dashed line) produces modest AP prolongation, consistent with the fact that outward current through I_{K1} is activated primarily at potentials which are hyperpolarized relative to the plateau potential. The most striking result is shown by the short-dashed line in Fig. 14C – significant AP prolongation occurs following down-regulation of SERCA2α. This down-regulation results in a near doubling of AP duration that is similar to that observed experimentally (Fig. 14A).

We have shown that the mechanism of this AP prolongation following down-regulation of SERCA2α involves tight coupling between Ca^{2+} release from the JSR and Ca^{2+}-dependent inactivation of LCCs. Decreases in JSR Ca^{2+} load produced by down-regulation of SERCA2α and up-regulation of NCX1 lead to reduced Ca^{2+} release into the dyadic space. This reduction of the subspace Ca^{2+} transient in turn produces a reduction of calcium-calmodulin (Ca^{2+}/CaM)-dependent inactivation of the L-type Ca^{2+} current. This reduction of inactivation increases the late component of the L-type Ca^{2+} current, prolonging AP duration. Thus, a fundamental hypothesis to emerge from these modeling studies is that tight coupling between JSR Ca^{2+} load, JSR Ca^{2+} release and L-type Ca^{2+} current mediated by Ca^{2+}/CaM-dependent inactivation of LCCs (as shown by the data of Fig. 3) is a critically important modulator of AP duration in HF.

4.2 A General Mechanism for Regulation of AP Duration

The results described above demonstrate that as a consequence of strong Ca^{2+}-dependent inactivation of LCCs by Ca^{2+} release through RyRs, disease processes producing an alteration of JSR Ca^{2+} levels can have a strong effect on AP shape and duration. Recent experimental data has provided more direct evidence that ablation of Ca^{2+}-dependent inactivation of LCCs has a profound effect on the AP. Figure 15A shows APs measured in wild-type (WT) guinea pig ventricular myoyctes versus myocytes in which Ca^{2+}-dependent

inactivation of LCCs is ablated by overexpression of a mutant CaM. AP duration in WT cells is approximately 200 ms, whereas that in cells expressing mutant CaM is well over 2500 ms. Figure 15B, obtained using the stochastic local control model, shows that this cellular phenotype is reproduced when Ca^{2+}-dependent inactivation of LCCs is ablated in the model.
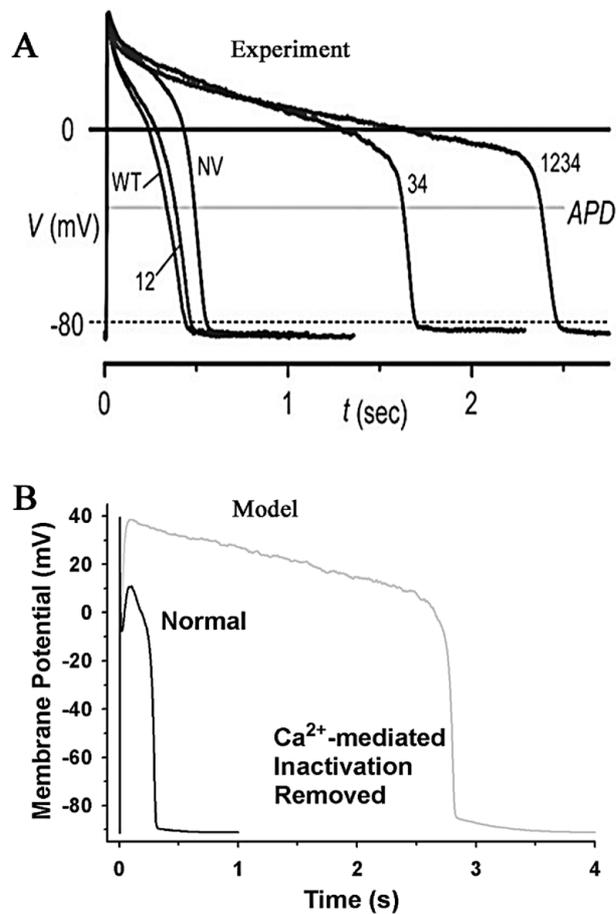

Fig. 15. (**A**) Normal guinea pig ventricular myocyte AP (labeled WT) versus AP measured in myocytes overexpressing muta5CaM (labeled 1234), thus ablating Ca^{2+}-dependent inactivation of LCCs. Reproduced from Fig. 3 of Alseikhan et al. [74], with permission. (**B**) APs simulated using the stochastic local control model with (*black line*) and without (*gray line*) Ca^{2+}-dependent inactivation of LCCs

5 Discussion

Results described in the previous sections indicate that as a result of the research efforts of many laboratories, both experimental investigation as well as mathematical and computational modeling of cardiac EC coupling processes has advanced rapidly. In the following discussion, we address three areas of modeling research which we believe hold particular promise for future development.

5.1 Regulation of Cardiac EC Coupling by Signaling Pathways

Activation of the β-adrenergic (β-AR) signaling pathway enhances cardiac function during stress or exercise through PKA-mediated phosphorylation of target proteins that are directly involved in the process of EC coupling. Targets include LCCs, the SR membrane protein phospholamban (PLB) and RyRs. PKA-mediated phosphorylation of LCCs increases both the fraction of channels available for gating as well as the fraction gating in mode 2 (a gating mode characterized by long-lasting channel openings). The resulting increase in L-type Ca^{2+} current boosts the trigger signal for CICR. Phosphorylation of PLB relieves its inhibitory regulation of the SERCA2α pump, thereby enhancing SR Ca^{2+} uptake, increasing JSR Ca^{2+} content and thus influencing LCC function through Ca^{2+}-dependent inactivation processes (for review, see Bers [66]). As discussed in Sect. 2.2.2, the functional role of PKA-mediated phosphorylation of RyR remains controversial.

Because of its central role in regulation of cardiac contractility, the development of reconstructive and predictive computational models of the β-AR signaling pathway, the actions of this signaling pathway on molecular targets and the consequences of these actions on myocyte function remains an important goal. First steps have been taken. Recently, Greenstein et al. [67] have developed computational models of the effects of PKA-induced phosphorylation of LCCs, PLB and RyRs. The stochastic local control model described in Sect. 3.2 was then used to investigate the ways in which these phosphorylation events regulate properties of EC coupling. Simulations results indicated that characteristic changes in the voltage-dependent EC coupling gain function may be attributed to phosphorylation-induced alterations of specific target proteins. PKA-induced phosphorylation of PLB and the resulting upregulation of SERCA2α activity increased EC coupling gain uniformly as a function of membrane potential by increasing JSR Ca^{2+} levels and thus RyR release flux, similar to the findings of Ginsburg and Bers [68]. Increased LCC open frequency produced a decrease in gain similar to that measured by Song et al. [54]. Increasing RyR Ca^{2+} sensitivity produced an increase in gain similar in shape to that measured by Viatchenko-Karpinski and Györke [69]. These model results suggest that differences in the effects of β-AR stimulation on experimental estimates of the EC coupling gain function reported in the literature may result from differences in the primary downstream targets of β-AR

signaling in each of these studies. They also showed that the phosphorylation-induced changes in LCC gating mode (increased gating in Mode 2) produced by either PKA of CaMKII could function to trigger arrhythmias known as early after-depolarizations [67]. Experimental resolution of the actions of β-AR signaling on molecular targets, especially the RyR, and the analysis of the consequences of these actions on the integrative function of the cardiac myoycte remains an important goal for future model development. In addition, Saucerman et al. [70] have recently developed an experimentally-based computational model of the cardiac β-AR signaling pathway. The integration of such signaling models with quantitative descriptions of the effects of phosphorylation of molecular targets, not only in response to PKA but to CaMKII as well, remains an additional future goal.

5.2 Dyadic Ca^{2+} Dynamics

A range of theoretical and computational models predict that Ca^{2+} concentration in the dyad rises to approximately 10–$100\,\mu m$ during the AP. A simple calculation shows that given the estimated dimensions of the dyad ($400\,nm$ diameter, $10\,nm$ depth), the number of Ca^{2+} ions yielding these estimated concentrations is very small indeed – a conservative estimate being 10–100 ions per dyad. This fact calls into question core assumptions of each of the three EC coupling models described in this chapter, namely, that Ca^{2+} levels in the dyad involved in triggering CICR may be represented using a single compartment of uniform concentration and that time-varying changes of Ca^{2+} concentration may be described using the laws of mass action. It may be the case that the random motion of Ca^{2+} ions within the space may contribute an important "noise" factor to interactions between RyRs and LCCs. Future modeling efforts must address this issue, making use of tools such as M-Cell (www.mcell.psc.edu) to describe the microenvironment within which the LCCs and RyRs interact as well as the trajectories of individual Ca^{2+} ions within that environment.

5.3 Localized Signaling within Molecular Complexes

Recordings from rat hippocampal neurons have demonstrated the existence of a pre-assembled macromolecular signaling complex which associates the β-AR with the LCC [71]. The complex also contains a G protein, an adenylyl cyclase, protein kinase A, and a phosphatase. It is also known that in cardiac myocytes, a kinase-anchoring protein 15 (AKAP15) co-immunoprecipitates with LCCs [72]. The physical association of the molecular components of β-AR signaling pathway elements suggests that the chain of signaling events from receptor-ligand binding to phosphorylation of the LCC will be determined by interactions between a small number of molecular entities within a highly localized micro-environment. Modeling studies of systems such as these may benefit from an approach which combines molecular dynamic, stochastic and

deterministic methods in order to maintain detailed descriptions of local molecular interactions. Furthermore, the need for implementing local molecular interactions poses a unique challenge to the scientific community. More mathematically efficient ways of describing local phenomena are necessary in order to build models that can be used to rapidly explore hypotheses and/or can be incorporated into larger scale multicellular tissue or whole organ models.

Acknowledgements

References

1. Feske, S., Giltnane, J., Dolmetsch, R., Staudt, L.M. and Rao, A., *Gene regulation mediated by calcium signals in T lymphocytes.* Nat Immunol, 2001. **2**: p. 316–24. 97
2. Lanahan, A. and Worley, P., *Immediate-early genes and synaptic function.* Neurobiol Learn Mem, 1998. **70**(1-2): p. 37–43. 97
3. Cortassa, S., Aon, M., Marban, E., Winslow, R. and O'Rourke, B., *An integrated model of cardiac mitochondrial energy metabolism and calcium dynamics.* Biophys. J., 2003. **84**: p. 2734–2755. 97
4. Brette, F. and Orchard, C., *T-tubule function in mammalian cardiac myocytes.* Circ Res, 2003. **92**(11): p. 1182–92. 98
5. Langer, G.A. and Peskoff, A., *Calcium concentration and movement in the diadic cleft space of the cardiac ventricular cell.* Biophys. J., 1996. **70**: p. 1169–1182. 99, 107
6. Bers, D.M. and Perez-Reyes, E., *Ca channels in cardiac myocytes: structure and function in Ca influx and intracellular Ca release.* Cardiovasc Res, 1999. **42**: p. 339–60. 99
7. Zhang, J.F., Ellinor, P.T., Aldrich, R.W. and Tsien, R.W., *Molecular determinants of voltage-dependent inactivation in calcium channels.* Nature, 1994. **372**(6501): p. 97–100. 99
8. Colecraft, H.M., Alseikhan, B., Takahashi, S.X., Chaudhuri, D., Mittman, S., Yegnasubramanian, V., Alvania, R.S., Johns, D.C., Marban, E. and Yue, D.T., *Novel functional properties of Ca^{2+} channel beta subunits revealed by their expression in adult rat heart cells.* J Physiol, 2002. **541**(Pt 2): p. 435–52. 99
9. 9. Kamp, T.J. and Hell, J.W., *Regulation of cardiac L-type calcium channels by protein kinase A and protein kinase C.* Circ Res, 2000. **87**(12): p. 1095–102. 100
10. Peterson, B., DeMaria, C., Adelman, J. and Yue, D., *Calmodulin is the Ca^{2+} sensor for Ca^{2+}-dependent inactivation of L-type calcium channels.* Neuron, 1999. **1999**: p. 549–558. 100, 101
11. Peterson, B.Z., Lee, J.S., Mulle, J.G., Wang, Y., Leon, M.d. and Yue, D.T., *Critical determinants of Ca^{2+}-dependent inactivation within an EF-hand motif of L-type Ca^{2+} channels.* Biophys. J., 2000. **78**: p. 1906–1920. 100

12. Linz, K.W. and Meyer, R., *Control of L-type calcium current during the action potential of guinea-pig ventricular myocytes.* J Physiol (Lond), 1998. **513**(Pt 2): p. 425–42. 101, 105, 106, 111

13. Lehnart, S.E., Wehrens, X.H., Kushnir, A. and Marks, A.R., *Cardiac ryanodine receptor function and regulation in heart disease.* Ann N Y Acad Sci, 2004. **1015**: p. 144–59. 102

14. Marx, S.O., Gaburjakova, J., Gaburjakova, M., Henrikson, C., Ondrias, K. and Marks, A., *Coupled gating between cardiac calcium release channels (ryanodine receptors).* Circ. Res., 2001. **88**: p. 1151–1158. 102, 119

15. Marx, S.O., Reiken, S., Hisamatsu, Y., Jayaraman, T., Burkhoff, D., Rosemblit, N. and Marks, A.R., *PKA phosphorylation dissociates FKBP12.6 from the calcium release channel (ryanodine receptor): defective regulation in failing hearts.* Cell, 2000. **101**: p. 365–76. 102

16. Xiao, B., Sutherland, C., Walsh, M.P. and Chen, S.R., *Protein kinase A phosphorylation at serine-2808 of the cardiac Ca^{2+}-release channel (ryanodine receptor) does not dissociate 12.6-kDa FK506-binding protein (FKBP12.6).* Circ Res, 2004. **94**: p. 487–95. 102

17. Wehrens, X.H., Lehnart, S.E., Reiken, S.R. and Marks, A.R., *Ca^{2+}/calmodulin-dependent protein kinase II phosphorylation regulates the cardiac ryanodine receptor.* Circ Res, 2004. **94**(6): p. e61–70. 102

18. Fabiato, A., *Time and calcium dependence of activation and inactivation of calcium-induced release of calcium from the sarcoplasmic reticulum of a skinned canine cardiac Purkinje cell.* J. Gen. Physiol., 1985. **85**: p. 247–289. 102

19. Fabiato, A., *Rapid ionic modifications during the aequorin-detected calcium transient in a skinned canine cardiac Purkinje cell.* J Gen Physiol, 1985. **85**: p. 189–246. 102

20. Fabiato, A., *Simulated calcium current can both cause calcium loading in and trigger calcium release from the sarcoplasmic reticulum of a skinned canine cardiac Purkinje cell.* J Gen Physiol, 1985. **85**: p. 291–320. 102

21. Wier, W.G., Egan, T.M., Lopez-Lopez, J.R. and Balke, C.W., *Local control of excitation-contraction coupling in rat heart cells.* J. Physiol., **474**: p. 463–471. 102, 103, 107, 116

22. Bers, D. and Stiffel, V., *Ratio of ryanodine to dihidropyridine receptors in cardiac and skeletal muscle and implications for E-C coupling.* Am. J. Physiol., 1993. **264**(6 Pt 1): p. C1587–C1593. 102

23. Langer, G.A., *Myocardial Ion Transporters*, in *The Myocardium*, G.A. Langer, Editor. 1997, Academic Press: San Diego. p. 143–179. 103

24. Blaustein, M.P. and Lederer, W.J., *Sodium/calcium exchange: its physiological implications.* Physiol Rev, 1999. **79**: p. 763–854. 103

25. Fujioka, Y., Komeda, M. and Matsuoka, S., *Stoichiometry of Na^+-Ca^{2+} exchange in inside-out patches excised from guinea-pig ventricular myocytes.* J Physiol, 2000. **523 Pt 2**: p. 339–51. 103

26. Kang, T.M., Markin, V.S. and Hilgemann, D.W., *Ion fluxes in giant excised cardiac membrane patches detected and quantified with ion-selective microelectrodes.* J Gen Physiol, 2003. **121**: p. 325–47. 103

27. Grantham, C.J. and Cannell, M.B., *Ca^{2+} influx during the cardiac action potential in guinea pig ventricular myocytes.* Circ. Res., 1996. **79**: p. 194–200. 103

28. Shannon, T.R., Ginsburg, K.S. and Bers, D.M. *Reverse mode of the SR Ca pump limits SR Ca uptake in permeabilized and voltage clamped myocytes.* in *Cardiac Sarcoplasmic Reticulum Function and Regulation of Contractility.* 1997. Washington, DC: New York Academy of Sciences. 104

29. Shannon, T.R., Ginsberg, K.S. and Bers, D.M., *SR Ca uptake rate in permeabilized ventricular myocytes is limited by reverse rate of the SR Ca pump.* Biophys. J., 1997. **72**: p. A167. 104

30. Stern, M., *Theory of excitation-contraction coupling in cardiac muscle.* Biophys J, 1992. **63**: p. 497–517. 104, 106, 107

31. Jafri, S., Rice, J.J. and Winslow, R.L., *Cardiac Ca^{2+} dynamics: The roles of ryanodine receptor adaptation and sarcoplasmic reticulum load.* Biophys. J., 1998. **74**: p. 1149–1168. 104, 105, 106, 108, 113, 114

32. Winslow, R.L., Rice, J.J., Jafri, M.S., Marban, E. and O'Rourke, B., *Mechanisms of Altered Excitation-Contraction Coupling in Canine Tachycardia-Induced Heart Failure. II. Model Studies.* Circ. Res., 1999. **84**: p. 571–586. 104, 105, 106, 108, 122, 123

33. Noble, D., Varghese, A., Kohl, P. and Noble, P., *Inproved Guinea-pig ventricular cell model incorporating a diadic space, Ikr and Iks, and length- and tension-dependent processes.* Can. J. Cardiol., 1998. **14**: p. 123–134. 104

34. Puglisi, J.L., Wang, F. and Bers, D.M., *Modeling the isolated cardiac myocyte.* Prog Biophys Mol Biol, 2004. **85**(2-3): p. 163–78. 104

35. Faber, G.M. and Rudy, Y., *Action potential and contractility changes in (i) overloaded cardiac myocytes: a simulation study.* Biophys J, 2000. **78**: p. 2392–404. 104

36. Luo, C.H. and Rudy, Y., *A dynamic model of the cardiac ventricular action potential: I. Simulations of ionic currents and concentration changes.* Circ Res, 1994. **74**: p. 1071–1096. 104, 105, 106

37. Priebe, L. and Beuckelmann, D.J., *Simulation study of cellular electric properties in heart failure.* Circ Res, 1998. **82**(11): p. 1206–23. 104

38. Rice, J.J., Jafri, M.S. and Winslow, R.L., *Modeling short-term interval-force relations in cardiac muscle.* Am J Physiol, 2000. **278**: p. H913. 105

39. Iyer, V., Mazhari, R. and Winslow, R.L., *A computational model of the human left-ventricular epicardial myocyte.* Biophys. J., 2004. **87**: p. in press. 105

40. Sham, J.S.K., *Ca^{2+} release-induced inactivation of Ca^{2+} current in rat ventricular myocytes: evidence for local Ca^{2+} signalling.* J. Physiol., 1997. **500**: p. 285–295. 107

41. Bers, D.M., *Excitation Contraction Coupling and Cardiac Contractile Force.* Series in Cardiovascular Medicine. Vol. 122. 1993, Boston: Kluwer Academic Press. 107

42. Franzini-Armstrong, C., Protasi, F. and Ramesh, V., *Shape, size, and distribution of Ca^{2+} release units and couplons in skeletal and cardiac muscles.* Biophys J, 1999. **77**: p. 1528–39. 107, 109

43. Rice, J.J., Jafri, M.S. and Winslow, R.L., *Modeling gain and gradedness of Ca^{2+} release in the functional unit of the cardiac diadic space.* Biophys J, 1999. **77**: p. 1871–84. 107, 108

44. Soeller, C. and Cannell, M.B., *Numerical simulation of local calcium movements during L-type calcium channel gating in the cardiac diad.* Bipphys. J., 1997. **73**: p. 97–111. 107

45. Cannell, M.B. and Soeller, C., *Numerical analysis of ryanodine receptor activation by L-type channel activity in the cardiac muscle diad.* Biophys. J., 1997. **73**: p. 112–122. 107

46. Stern, M.D., Song, L.S., Cheng, H., Sham, J.S., Yang, H.T., Boheler, K.R. and Rios, E., *Local control models of cardiac excitation-contraction coupling. A possible role for allosteric interactions between ryanodine receptors.* J Gen Physiol, 1999. **113**: p. 469–89. 107, 114

47. Greenstein, J.L. and Winslow, R.L., *An integrative model of the cardiac ventricular myocyte incorporating local control of Ca^{2+} release.* Biophys J, 2002. **83**(6): p. 2918–45. 108, 110, 113, 115, 118, 119, 120

48. Mazhari, R., Greenstein, J.L., Winslow, R.L., Marban, E. and Nuss, H.B., *Molecular interactions between two long-QT syndrome gene products, HERG and KCNE2, rationalized by in vitro and in silico analysis.* Circ Res, 2001. **89**: p. 33–8. 108

49. Greenstein, J., Po, S., Wu, R., Tomaselli, G. and Winslow, R.L., *Role of the calcium-independent transient outward current Ito1 in action potential morphology and duration.* Circ. Res., 2000. **87**: p. 1026. 108, 123

50. Keizer, J., Smith, G.D., Ponce-Dawson, S. and Pearson, J.E., *Saltatory propagation of Ca^{2+} waves by Ca^{2+} sparks.* Biophys J, 1998. **75**: p. 595–600. 108

51. Wang, S.Q., Song, L.S., Lakatta, E.G. and Cheng, H., *Ca^{2+} signalling between single L-type Ca^{2+} channels and ryanodine receptors in heart cells.* Nature, 2001. **410**(6828): p. 592–6. 108, 115, 119

52. Parker, I., Zang, W.J. and Wier, W.G., *Ca^{2+} sparks involving multiple Ca^{2+} release sites along Z-lines in rat heart cells.* J Physiol (Lond), 1996. **497**(Pt 1): p. 31–8. 108

53. Song, L.S., Sham, J.S., Stern, M.D., Lakatta, E.G. and Cheng, H., *Direct measurement of SR release flux by tracking 'Ca^{2+} spikes' in rat cardiac myocytes.* J Physiol, 1998. **512 (Pt 3)**: p. 677–91. 108

54. Song, L.S., Wang, S.Q., Xiao, R.P., Spurgeon, H., Lakatta, E.G. and Cheng, H., *beta-Adrenergic Stimulation Synchronizes Intracellular Ca^{2+} Release During Excitation-Contraction Coupling in Cardiac Myocytes.* Circ Res, 2001. **88**(8): p. 794–801. 109, 125

55. Matsumoto, M. and Nishimura, T., *Mersenne twister: A 623-dimensionally equidistributed uniform pseudo-random number generator.* ACMTMCS, 1998. **8**: p. 3–30. 110

56. Hinch, R., Greenstein, J.L., Tanskanen, A.J. and Winslow, R.L., *A simplified local control model of calcium induced calcium release in cardiac ventricular myocytes.* Biophys. J., 2004. **87**: p. 3723–3736. 112, 114

57. Hinch, R., *A mathematical analysis of the generation and termination of calcium sparks.* Biophys J, 2004. **86**: p. 1293–307. 112, 113, 115

58. Sobie, E.A., Dilly, K.W., dos Santos Cruz, J., Lederer, W.J. and Jafri, M.S., *Termination of cardiac Ca^{2+} sparks: an investigative mathematical model of calcium-induced calcium release.* Biophys J, 2002. **83**: p. 59–78. 115

59. Shannon, T.R., Guo, T. and Bers, D.M., *Ca^{2+} scraps: local depletions of free in cardiac sarcoplasmic reticulum during contractions leave substantial Ca^{2+} reserve.* Circ Res, 2003. **93**: p. 40–5. 115

60. Zahradnikova, A., Kubalova, Z., Pavelkova, J., Gyorke, S. and Zahradnik, I., *Activation of calcium release assessed by calcium release-induced inactivation of calcium current in rat cardiac myocytes.* Am J Physiol Cell Physiol, 2004. **286**: p. C330–41. 117

61. Beuckelmann, D.J., Nabauer, M. and Erdmann, E., *Alterations of K^+ currents in isolated human ventricular myocytes from patients with terminal heart failure.* Circ. Res., **73**: p. 379–385. 121

62. Kaab, S., Nuss, H.B., Chiamvimonvat, N., O'Rourke, B., Pak, P.H., Kass, D.A., Marban, E. and Tomaselli, G.F., *Ionic mechanism of action potential prolongation in ventricular myocytes from dogs with pacing-induced heart failure.* Circ Res, 1996. **78**: p. 262–273. 121

63. Näbauer, M., Beuckelmann, D.J., Überfuhr, P. and Steinbeck, G., *Regional differences in current density and rate-dependent properties of the transient outward current in subepicardial and subendocardial myocytes of human left ventricle.* Circulation, 1996. **93**: p. 168–177. 121

64. O'Rourke, B., Peng, L.F., Kaab, S., Tunin, R., Tomaselli, G.F., Kass, D.A. and Marban, E., *Mechanisms of altered excitation-contraction coupling in canine tachycardia-induced heart: Experimental studies.* Circ. Res., 1999. **84**: p. 562–570. 121

65. Winslow, R., Greenstein, J., Tomaselli, G. and O'Rourke, B., *Computational model of the failing myocyte: Relating altered gene expression to cellular function.* Phil. Trans. Roy. Soc. Lond. A, 2001. **359**: p. 1187–1200. 123

66. Bers, D.M., *Cardiac excitation-contraction coupling.* Nature, 2002. **415**(6868): p. 198–205. 99, 125

67. Greenstein, J.L., Tanskanen, A.J. and Winslow, R.L., *Modeling the actions of b-adrenergic signaling on excitation-contraction coupling processes.* Ann. N. Y. Acad. Sci., 2004. **1015**: p. 16–27. 125, 126

68. Ginsburg, K.S., Weber, C.R. and Bers, D.M., *Control of maximum sarcoplasmic reticulum Ca load in intact ferret ventricular myocytes. Effects of thapsigargin and isoproterenol.* J Gen Physiol, 1998. **111**: p. 491–504. 125

69. Viatchenko-Karpinski, S. and Gyorke, S., *Modulation of the Ca^{2+}-induced Ca^{2+} release cascade by {beta}-adrenergic stimulation in rat ventricular myocytes.* J Physiol (Lond), 2001. **533**: p. 837–848. 125

70. Saucerman, J.J., Brunton, L.L., Michailova, A.P. and McCulloch, A.D., *Modeling beta-adrenergic control of cardiac myocyte contractility in silico.* J Biol Chem, 2003. **278**(48): p. 47997–8003. 126

71. Davare, M.A., Avdonin, V., Hall, D.D., Peden, E.M., Burette, A., Weinberg, R.J., Horne, M.C., Hoshi, T. and Hell, J.W., *A beta2 adrenergic receptor signaling complex assembled with the Ca^{2+} channel Cav1.2.* Science, 2001. **293**(5527): p. 98–101. 126

72. Hulme, J.T., Lin, T.W., Westenbroek, R.E., Scheuer, T. and Catterall, W.A., *Beta-adrenergic regulation requires direct anchoring of PKA to cardiac CaV1.2 channels via a leucine zipper interaction with A kinase-anchoring protein 15.* Proc Natl Acad Sci U S A, 2003. **100**(22): p. 13093–8. 126

73. Katz, A.M., *Physiology of the Heart.* Second ed. 1992, New York: Raven Press. 98

74. Alseikhan, B.A., DeMaria, C.D., Colecraft, H.M. and Yue, D.T., *Engineered calmodulins reveal the unexpected eminence of Ca^{2+} channel inactivation in controlling heart excitation.* Proc Natl Acad Sci U S A, 2002. **99**(26): p. 17185–90. 124